



# Volatility and lifetime against OH heterogeneous reaction of ambient isoprene-epoxydiols-derived secondary organic aerosol (IEPOX-SOA)

Weiwei Hu<sup>1,2</sup>, Brett B. Palm<sup>1,2</sup>, Douglas A. Day<sup>1,2</sup>, Pedro Campuzano-Jost<sup>1,2</sup>, Jordan E. Krechmer<sup>1,2</sup>, Zhe Peng<sup>1,2</sup>, Suzane S. de Sá<sup>3</sup>, Scot T. Martin<sup>3,4</sup>, M. Lizabeth Alexander<sup>5</sup>, Karsten Baumann<sup>6</sup>, Lina Hacker<sup>7</sup>, Astrid Kiendler-Scharr<sup>7</sup>, Abigail R. Koss<sup>1,2,8</sup>, Joost A. de Gouw<sup>1,2,8</sup>, Allen H. Goldstein<sup>9,10</sup>, Roger Seco<sup>11</sup>, Steven J. Sjostedt<sup>8</sup>, Jeong-Hoo Park<sup>12</sup>, Alex B. Guenther<sup>11</sup>, Saewung Kim<sup>11</sup>, Francesco Canonaco<sup>13</sup>, André S. H. Prévôt<sup>13</sup>, William H. Brune<sup>14</sup>, and Jose L. Jimenez<sup>1,2</sup>

<sup>1</sup>Cooperative Institute for Research in Environmental Sciences, University of Colorado, Boulder, CO 80309, USA

<sup>2</sup>Department of Chemistry and Biochemistry, University of Colorado, Boulder, CO 80309, USA

<sup>3</sup>John A. Paulson School of Engineering and Applied Sciences Harvard University, Cambridge, MA 01742, USA

<sup>4</sup>Department of Earth and Planetary Sciences, Harvard University, Cambridge, MA 01742, USA

<sup>5</sup>Environmental Molecular Sciences Laboratory, Pacific Northwest National Laboratory, Richland, WA 99352, USA

<sup>6</sup>Atmospheric Research and Analysis Inc., Morrisville, NC 27560, USA

<sup>7</sup>Institute for Energy and Climate Research – Troposphere (IEK-8), Forschungszentrum Jülich, 52425 Jülich, Germany

<sup>8</sup>Earth System Research Laboratory, NOAA, Boulder, CO 80305, USA

<sup>9</sup>Department of Environmental Science, Policy, and Management, University of California, Berkeley, CA 94720, USA

<sup>10</sup>Department of Civil and Environmental Engineering, University of California, Berkeley, CA 94720, USA

<sup>11</sup>Department of Earth System Science, University of California, Irvine, CA 92697, USA

<sup>12</sup>National Institute of Environmental Research, Incheon 22689, Republic of Korea

<sup>13</sup>Laboratory of Atmospheric Chemistry, Paul Scherrer Institute (PSI), 5232 Villigen, Switzerland

<sup>14</sup>Department of Meteorology, Pennsylvania State University, University Park, PA 16802, USA

Correspondence to: J. L. Jimenez (jose.jimenez@colorado.edu)

Received: 17 May 2016 – Published in Atmos. Chem. Phys. Discuss.: 23 May 2016

Revised: 1 September 2016 – Accepted: 2 September 2016 – Published: 19 September 2016

**Abstract.** Isoprene-epoxydiols-derived secondary organic aerosol (IEPOX-SOA) can contribute substantially to organic aerosol (OA) concentrations in forested areas under low NO conditions, hence significantly influencing the regional and global OA budgets, accounting, for example, for 16–36 % of the submicron OA in the southeastern United States (SE US) summer. Particle evaporation measurements from a thermodynamic show that the volatility of ambient IEPOX-SOA is lower than that of bulk OA and also much lower than that of known monomer IEPOX-SOA tracer species, indicating that IEPOX-SOA likely exists mostly as oligomers in the aerosol phase. The OH aging process of ambient IEPOX-SOA was investigated with an oxidation flow reactor (OFR). New IEPOX-SOA formation in the reactor was negligible, as the OFR does not accelerate processes such as aerosol up-

take and reactions that do not scale with OH. Simulation results indicate that adding  $\sim 100 \mu\text{g m}^{-3}$  of pure  $\text{H}_2\text{SO}_4$  to the ambient air allows IEPOX-SOA to be efficiently formed in the reactor. The heterogeneous reaction rate coefficient of ambient IEPOX-SOA with OH radical ( $k_{\text{OH}}$ ) was estimated as  $4.0 \pm 2.0 \times 10^{-13} \text{ cm}^3 \text{ molec}^{-1} \text{ s}^{-1}$ , which is equivalent to more than a 2-week lifetime. A similar  $k_{\text{OH}}$  was found for measurements of OH oxidation of ambient Amazon forest air in an OFR. At higher OH exposures in the reactor ( $> 1 \times 10^{12} \text{ molec cm}^{-3} \text{ s}$ ), the mass loss of IEPOX-SOA due to heterogeneous reaction was mainly due to revolatilization of fragmented reaction products. We report, for the first time, OH reactive uptake coefficients ( $\gamma_{\text{OH}} = 0.59 \pm 0.33$  in SE US and  $\gamma_{\text{OH}} = 0.68 \pm 0.38$  in Amazon) for SOA under ambient conditions. A relative humidity dependence of  $k_{\text{OH}}$

and  $\gamma_{\text{OH}}$  was observed, consistent with surface-area-limited OH uptake. No decrease of  $k_{\text{OH}}$  was observed as OH concentrations increased. These observations of physicochemical properties of IEPOX-SOA can help to constrain OA impact on air quality and climate.

## 1 Introduction

Organic aerosol (OA), which comprises 10–90 % of ambient submicron aerosol mass globally, has important impacts on climate forcing and human health (Kanakidou et al., 2005; Zhang et al., 2007; Hallquist et al., 2009). However, quantitative predictions of OA mass concentrations often fail to match the real ambient measurements by large factors, (e.g., Volkamer et al., 2006; Dzepina et al., 2011; Tsigaridis et al., 2014). Improved characterization of the properties and lifetime of OA is needed to better constrain OA model predictions.

Isoprene is the most abundant non-methane hydrocarbon (NMHC) emitted into the Earth's atmosphere (Guenther et al., 2012). Many studies in the past decade have shown that the reaction products of isoprene-derived epoxydiols (IEPOX), formed under low NO conditions (Paulot et al., 2009), can contribute efficiently to secondary OA (SOA) via reactive uptake of gas-phase IEPOX onto acidic aerosols (Eddingsaas et al., 2010; Froyd et al., 2010; Surratt et al., 2010; Lin et al., 2012; Liao et al., 2015). IEPOX-SOA measurements in field studies show that it can account for 6–34 % of total OA over multiple forested areas across the globe, with important impacts on the global and regional OA budget (Hu et al., 2015, and references therein). Although the formation of IEPOX-SOA from gas-phase IEPOX has been investigated in many laboratory studies (e.g., Eddingsaas et al., 2010; Lin et al., 2012; Gaston et al., 2014; Riedel et al., 2015), the lifetime and aging of IEPOX-SOA in the aerosol phase is still mostly unexplored in the literature.

IEPOX-SOA can be measured by multiple methods. Gas chromatography–mass spectrometry (GC–MS) or liquid chromatography–mass spectrometry (LC–MS) of filter extracts can be used to measure some IEPOX-SOA species (accounting for 8–80 % of total IEPOX-SOA depending on the study, Lin et al., 2012; Budisulistiorini et al., 2015; Hu et al., 2015). Recently, several studies have shown that factor analysis of real-time aerosol mass spectrometer (AMS) data provides a method to obtain the total amount, overall fraction contribution, and properties of IEPOX-SOA (Robinson et al., 2011; Budisulistiorini et al., 2013; Chen et al., 2015). The  $\text{C}_5\text{H}_6\text{O}^+$  ion at  $m/z$  82 in AMS spectra, arising from decomposition and ionization of molecular IEPOX-SOA species, has also been suggested as a proxy for real-time estimation of IEPOX-SOA (Hu et al., 2015).

The heterogeneous reaction of OA with hydroxyl radicals (OH) is a contributor to aerosol aging, and it significantly in-

fluences aerosol lifetime (George and Abbatt, 2010; George et al., 2015; Kroll et al., 2015). To describe the aging process, OA reaction rate coefficients with OH radicals ( $k_{\text{OH}}$ ), or alternatively, uptake coefficients of OH ( $\gamma_{\text{OH}}$ ), defined as the fraction of OH collisions with a compound that result in reaction, have been reported for numerous laboratory studies. Values of effective  $\gamma_{\text{OH}}$  ( $\leq 0.01$  to  $\geq 1$ ) also can vary significantly under different reaction conditions, such as different OA species (George and Abbatt, 2010), temperature and humidity (Park et al., 2008; Liu et al., 2012; Slade and Knopf, 2014), OH concentrations (Slade and Knopf, 2013; Arangio et al., 2015), and particle phase state or coatings (McNeill et al., 2008; Arangio et al., 2015). Most of the studies that have reported  $k_{\text{OH}}$  and  $\gamma_{\text{OH}}$  are based on laboratory experiments, with few experimental determinations of  $k_{\text{OH}}$  based on field measurements under ambient conditions (Slowik et al., 2012; Ortega et al., 2016), while no  $\gamma_{\text{OH}}$  has been reported based on field studies to our knowledge.

During the Southern Oxidant and Aerosol Study (SOAS), 17 % of ambient OA was estimated to be IEPOX-SOA (Hu et al., 2015). In this study, ambient gas and aerosol species were sampled through an oxidation flow reactor (OFR) and a thermodenuder (TD) to investigate heterogeneous oxidation and evaporation of ambient IEPOX-SOA, respectively. These systems included an AMS and other online instruments measuring both gas and aerosol species inflow and outflow. A simplified box model is used to investigate the fate of gas-phase IEPOX under ambient and OFR conditions. The potential of evaporation to impact the lifetime of IEPOX-SOA was evaluated. The heterogeneous reaction rate coefficient ( $k_{\text{OH}}$ ) and OH uptake coefficient ( $\gamma_{\text{OH}}$ ) of IEPOX-SOA with OH radicals are estimated from the OFR data. IEPOX-SOA aging during the dry season of 2014 in central Amazonia as part of the Green Ocean Amazon (GoAmazon2014/5, IOP2) experiment, using the same OFR experimental setup, was compared to the SOAS results.

## 2 Experimental method

### 2.1 Background and instrumentation

The SOAS study (hereafter referred to as the “SE US study”) took place in the southeastern United States (SE US) in the summer (1 June–15 July) of 2013. Results shown here are from the SEARCH Centreville Supersite (CTR) in a mixed forest in Alabama (32.95° N, 87.13° W; Hansen et al., 2003). The average ( $\pm$ standard deviation) temperature and relative humidity (RH) of ambient air were  $25 \pm 4^\circ$  and  $83 \pm 18\%$ , respectively (Fig. S1 in the Supplement). Biogenic volatile organic compounds (BVOCs) were highly abundant, with average isoprene and monoterpene concentrations of  $3.3 \pm 2.4$  and  $0.7 \pm 0.4$  ppb, respectively, and they displayed clear diurnal variations (Fig. S1). Isoprene showed a broad mid-afternoon peak ( $\sim 5.8$  ppb), and monoterpenes peaked during

the nighttime and early morning ( $\sim 0.9$ – $1.0$  ppb). Chemically resolved mass concentrations of submicron non-refractory aerosol ( $PM_{10}$ ) were measured by a high-resolution time-of-flight AMS (HR-ToF-AMS, Aerodyne Research Inc., Decarlo et al., 2006) at a time resolution of 2 min. Detailed information about AMS setup, operation, and data analysis is given in the supporting information as well as in Hu et al. (2015).

A Potential Aerosol Mass oxidation flow reactor (OFR) was used to investigate OA formation/aging from ambient air over a wide range of OH exposures ( $10^{10}$ – $10^{13}$  molec  $cm^{-3}$  s). This field-deployable OFR provides a fast and direct way to investigate oxidation processes of ambient gas and aerosol with OH radicals under low-NO chemistry (Kang et al., 2007; Lambe et al., 2011; R. Li et al., 2015; Peng et al., 2015; Ortega et al., 2016; Palm et al., 2016). The OFR is a cylindrical vessel ( $\sim 13$  L) with an average residence time of  $\sim 180$ – $220$  s in this study, depending on the flow rates of sampled ambient air ( $3.5$ – $4.2$  L  $min^{-1}$ ) (Figs. S2–S3). In the “OFR185” method of OH production used in this study, two low-pressure mercury lamps inside the OFR produce UV radiation at 185 and 254 nm (Peng et al., 2015). OH radicals were generated when the UV light initiated  $O_2$ ,  $H_2O$ , and  $O_3$  photochemistry (R. Li et al., 2015).

A large range of OH exposures ( $10^{10}$ – $10^{13}$  molec  $cm^{-3}$  s) can be achieved by varying UV light intensity, equivalent to several hours to several weeks of photochemical aging of ambient air (assuming a 24 h average OH =  $1.5 \times 10^6$  molec  $cm^{-3}$ ; Mao et al., 2009). Thus we believe that the range of OH exposures ( $10^{10}$ – $10^{13}$  molec  $cm^{-3}$  s) covered by our study is the relevant range for the atmosphere. We note that OH radical concentration can be calculated as the ratio of the OH exposure ( $10^{10}$ – $10^{13}$  molec  $cm^{-3}$  s) and the residence time (200 s). The calculated OH radical concentration in our flow reactor is between  $5 \times 10^7$  to  $5 \times 10^{10}$  molec  $cm^{-3}$ . The lower range of OH radical concentration is comparable to the higher end of observed ambient OH concentrations (Mao et al., 2009).

OH exposures in the OFR were calculated by the real-time decay of CO added to the ambient air in the OFR (1–2 ppm; OH reactivity  $\approx 5$ – $10$   $s^{-1}$ ). The empirical estimation of OH exposure based on the OFR output parameters  $O_3$ , water, and ambient OH reactivity ( $15$   $s^{-1}$ ) showed good agreement with that calculated from CO decay as shown in Fig. S4. The uncertainty of calculated OH exposures in the OFR was estimated as 35% based on regression analysis (R. Li et al., 2015; Peng et al., 2015).

The average wall loss corrections for OA in OFR during the SE US study is  $2 \pm 0.7$ %. This wall loss is estimated by comparing the ambient OA concentrations to those concentrations after the OFR when the UV lights were off and no oxidant was present (other than ambient  $O_3$ ).

A TD was used to investigate the volatility of ambient OA and IEPOX-SOA. The temperature in the TD increased linearly during the heating period (from 30 to 250° over 60 min)

and then cooled down to 30° for 60 min. More detailed information on the TD technique and instrumentation can be obtained elsewhere (Faulhaber et al., 2009; Huffman et al., 2009a, b).

A typical sampling cycle during the SE US study took a total of 24 min, sequentially sampling ambient air (4 min), TD (4 min), ambient air (4 min), OFR with OH radicals as oxidant (4 min), ambient air (4 min), and OFR with other types of oxidation (e.g.,  $O_3$  or  $NO_3$  as oxidants; 4 min), as illustrated in the diagram in Fig. S2. Only OFR data for OH oxidation using OFR185 method are presented here. A comparison of results from the OFR185 and OFR254 methods for a study at a pine forest was presented by Palm et al. (2016), showing similar SOA formation by both methods. Their results, together with modeling studies (Peng et al., 2015, 2016), showed that the OFR185 method is preferable for ambient studies, and thus that was the method used during the SE US study. UV light intensities in the OFR were changed immediately after sampling the second OFR outflow for each cycle. Thus, oxidant concentrations in the OFR had sufficient time (at least 12 min, i.e. 3–4 flow  $e$ -folding times) to stabilize before the next OFR sampling interval. The air from each sampling mode was sampled by the AMS, a scanning mobility particle sizer (for measuring particle number size distributions; SMPS, TSI Inc.), and several other instruments to measure related gas-phase species, e.g., VOCs from a proton-transfer-reaction mass spectrometer (PTR-MS),  $O_3$ , CO, and  $H_2O$  (Table S1 in the Supplement).

Measurements collected during the second Intensive Operating Period (IOP2) of the Green Ocean Amazon (GoAmazon2014/5, hereinafter “Amazon study”) Experiment (Martin et al., 2016), which took place in the dry season of central Amazonia, are also presented here. The region has high isoprene and monoterpene emissions (Karl et al., 2007; Martin et al., 2010). In this analysis, data from the “T3” ground site ( $3.213^\circ$  S,  $60.599^\circ$  W), a rural location 60 km west of Manaus (population 2 million), in the dry season (15 August to 15 October 2014) are also shown. Unlike the SE US study, the aerosols in the dry season of the Amazon study were heavily influenced by biomass burning (Martin et al., 2016), thus providing a difference dataset to investigate the IEPOX-SOA heterogeneous reaction. The instrument setup, OFR settings, sampling schemes, and data processing were similar to those for the SE US study.

## 2.2 IEPOX-SOA identification

We classified ambient OA using positive matrix factorization (PMF) on the time series of peak-fitted, high-resolution organic spectra measured by the AMS (Ulbrich et al., 2009). A factor corresponding to ambient IEPOX-SOA was assigned based on its spectral features (e.g., prominent  $C_5H_6O^+$  ion at  $m/z$  82), and strong correlation with hourly or daily measured 2-methyltetrols ( $R = 0.79$ ), an oxidation product of isoprene oxidation via the IEPOX pathway (Surratt et al.,

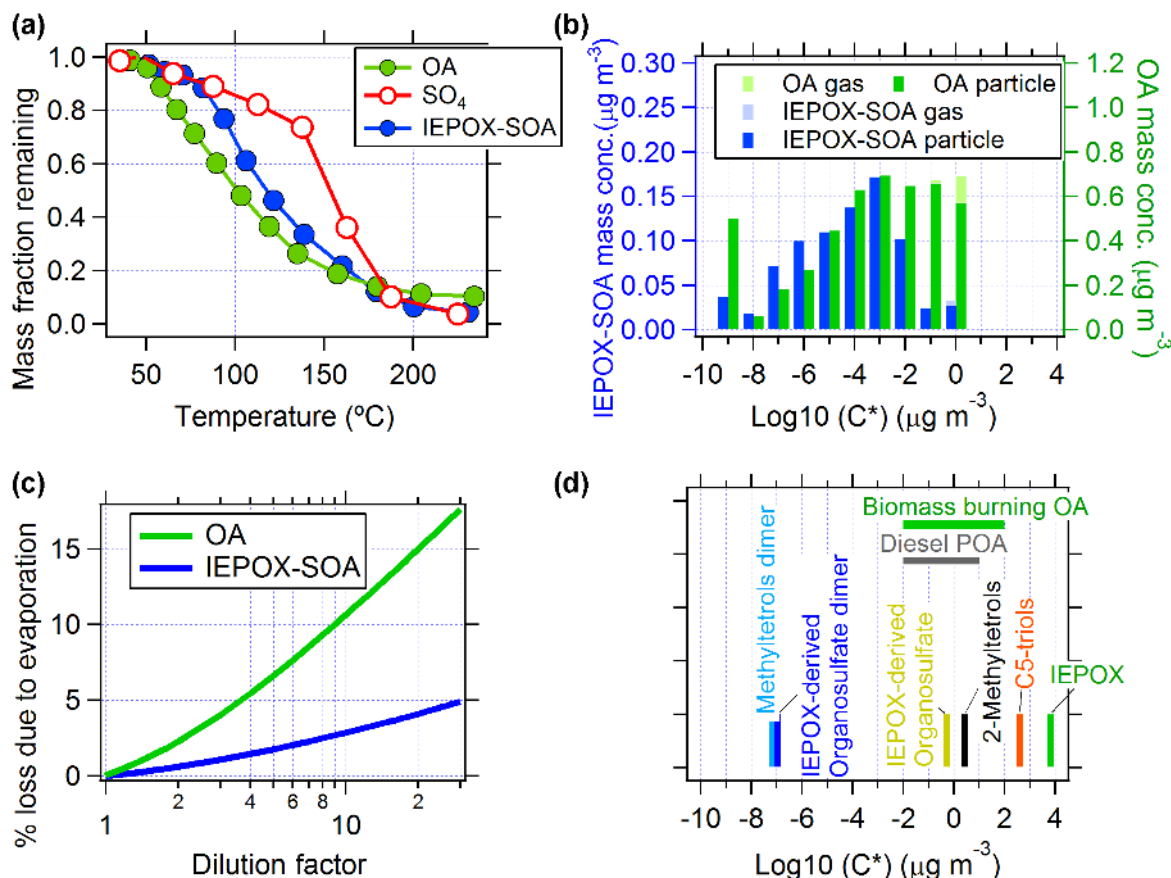


**Figure 1.** (a) Mean mass fraction remaining of IEPOX-SOA, OA, and SO<sub>4</sub> vs. temperature in TD “thermograms” during the SE US study. (b) Volatility distributions of IEPOX-SOA and OA estimated from TD thermograms (see text). Bars are offset for clarity and were both calculated for integer log( $C^*$ ) values. (c) Evaporation losses of IEPOX-SOA and OA as a function of dilution factors. (d) Volatility of typical IEPOX-SOA molecular species in the aerosol phase based on the SIMPOL group contribution method (Pankow and Asher, 2008). The reduction in vapor pressure upon addition of a nitrate group was used to estimate the effect of the sulfate group, due to lack of SIMPOL parameters for the latter, and the derived  $C^*$  may be overestimated for this reason.

2010; Hu et al., 2015), as well as with sulfate ( $R = 0.75$ ), which facilitates IEPOX-SOA formation through direct reactions or nucleophilic effects (T. B. Nguyen et al., 2014; Liao et al., 2015). Unconstrained PMF analysis often fails when the factor fractions become too small ( $< 5\%$ ), e.g., as is the case for the IEPOX-SOA at higher OH exposures in the OFR in this study (Ulbrich et al., 2009). To overcome this, a more advanced algorithm, the Multilinear Engine (ME-2) (Paatero, 2007; Canonaco et al., 2013), was applied through the recently implemented Source Finder (SoFi, Canonaco et al., 2013). In SoFi, the mass spectrum of the IEPOX-SOA factor was constrained based on the ambient spectrum of IEPOX-SOA from conventional PMF, and the concentrations of IEPOX-SOA factors were retrievable even at low concentrations. More information can be found in the Supplement (Sect. 2 and Figs. S5–S9). Hereafter we will abbreviate the IEPOX-SOA PMF factor as IEPOX-SOA.

In this study,  $C_5H_6O^+$  data directly measured from AMS are used as a complementary tool to examine/interpret the

analysis results from the IEPOX-SOA PMF factor, since both lab and ambient results have shown that  $C_5H_6O^+$  is a very good tracer for IEPOX-SOA (Robinson et al., 2011; Lin et al., 2012; Allan et al., 2014; Hu et al., 2015). Analyzing  $C_5H_6O^+$  is an easy alternative method to evaluate the physicochemical evolution of IEPOX-SOA, which avoids the uncertainties related to PMF analysis, and thus provides further confidence in the results. This is especially true when periods where the OA is dominated by IEPOX-SOA are analyzed.

### 2.3 Box model to simulate gas-phase IEPOX

The chemistry of OH oxidation in the OFR is typical of low-NO conditions, with HO<sub>2</sub> being the dominant reaction partner of RO<sub>2</sub> radicals due to the greatly elevated HO<sub>2</sub> concentrations and the very short lifetime of NO and NO<sub>x</sub> in OFR (R. Li et al., 2015; Peng et al., 2015). A box model (KinSim 3.2 in Igor Pro. 6.37) was used to simulate the fate of gas-phase IEPOX under both ambient and

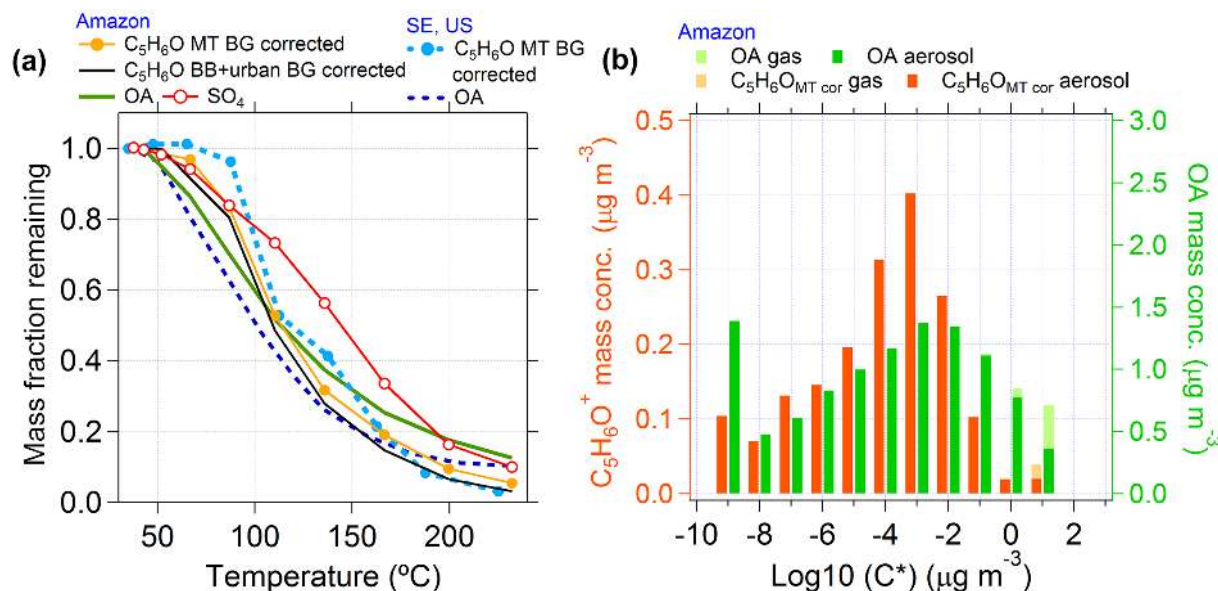


**Figure 2.** (a) Thermogram of OA, SO<sub>4</sub>, and background-corrected C<sub>5</sub>H<sub>6</sub>O<sup>+</sup> ion in the SE US and Amazon studies. (b) Volatility distributions of C<sub>5</sub>H<sub>6</sub>O<sup>+</sup> and OA estimated based on TD thermograms from the Amazon study.

OFR conditions, as shown in Fig. 3 (Paulot et al., 2009; Xie et al., 2013; Bates et al., 2014; Krechmer et al., 2015). A detailed description, including reactions and parameters in the model, pH-dependent uptake coefficient of IEPOX onto aerosols ( $\gamma_{\text{IEPOX}}$ ), aerosol surface area calculations, and estimated photolysis of IEPOX, can be found in the Supplement, Sect. S3 (Tables S2–3 and Figs. S10–14).

### 3 Results and discussion

#### 3.1 Low volatility of IEPOX-SOA

TDs are widely used to investigate the volatility distribution of OA in ambient air (e.g., Faulhaber et al., 2009; Cappa and Jimenez, 2010). IEPOX-SOA evaporates more slowly upon heating (Fig. 1a) than total OA over a very wide range of TD temperatures ( $< 170^\circ$ ), indicating that IEPOX-SOA has a lower volatility than bulk OA. Consistent with that result, a lower volatility of the IEPOX-SOA tracer C<sub>5</sub>H<sub>6</sub>O<sup>+</sup> in both SE US and Amazon studies was also found (Fig. 2).

The volatility distributions of IEPOX-SOA and OA were estimated following the method of Faulhaber et al. (2009), based on calibration of the relationship between TD temperature and organic species saturation concentration at 298 K ( $C^*$ ). Similar methods have been developed for other thermal desorption instruments (e.g., Chattopadhyay and Ziemann, 2005; Lopez-Hilfiker et al., 2016). The volatility distribution of IEPOX-SOA (Fig. 1b) shows mass peaks at  $C^* = 10^{-4}$ – $10^{-3} \mu\text{g m}^{-3}$ , which are much lower than those of diesel primary OA (POA;  $C^* = 10^{-2}$ – $1 \mu\text{g m}^{-3}$ ) and biomass-burning POA ( $C^* = 10^{-2}$ – $100 \mu\text{g m}^{-3}$ , Fig. 1d) at various OA con-

centrations ( $1$ – $100 \mu\text{g m}^{-3}$ ). Those types of POA are reported to be semivolatile (Cappa and Jimenez, 2010; Ranjan et al., 2012; May et al., 2013). The estimated distribution implies that very little of the ambient IEPOX-SOA was actively partitioning to the gas phase during SE US study (Fig. 1b). Although we cannot rule out some chemical changes during TD heating, this conclusion is dictated by the data at the lowest TD temperatures, when such chemistry is less likely. Lopez-Hilfiker et al. (2016) have shown that oligomer decomposition for IEPOX-SOA upon heating at  $\sim 90^\circ$  was important during the SE US study, but that process will only make the measured volatility of IEPOX-SOA in TD higher than it should be. This reinforces our conclusion about the low volatility of ambient IEPOX-SOA, consistent with the independent results of Lopez-Hilfiker et al. (2016).

Several molecular species (e.g., 2-methyltetrols, C<sub>5</sub>-alkene triols, IEPOX organosulfate and its dimer) comprising IEPOX-SOA have been characterized both in field and chamber studies (Surratt et al., 2010; Lin et al., 2012; Budisulistiorini et al., 2013; Liao et al., 2015). At the CTR site during the SE US study, 2-methyltetrols, C<sub>5</sub>-alkene triols, and IEPOX organosulfate measured by GC/MS and LC/MS in the particle phase accounted for an average of 80 % (individually 29, 28 and 24 %, respectively) of total IEPOX-SOA factor mass (Hu et al., 2015). The volatilities of these IEPOX-SOA molecular species were estimated based on the SIMPOL group contribution method (Pankow and Asher, 2008). The species reported to comprise most of IEPOX-SOA have relatively high  $C^*$  (2-methyltetrol =  $2.7 \mu\text{g m}^{-3}$ ; C<sub>5</sub>-alkene triols =  $400 \mu\text{g m}^{-3}$ , and IEPOX organosulfate =  $0.5 \mu\text{g m}^{-3}$ ). The alkene triols



in ambient air during the SE US study (where average OA mass concentration was  $3.6 \mu\text{g m}^{-3}$ ) should have been almost completely in the gas phase ( $> 98\%$ ), while 43 and 12 % of the methyltetrol and organosulfate should have been in the gas phase, respectively. The  $C^*$  of those monomer species is much higher than for the bulk IEPOX-SOA ( $C^* = 10^{-6} - 10^{-2} \mu\text{g m}^{-3}$ ) that they are thought to comprise. On the other hand, the estimated  $C^*$  of a hypothetical methyltetrol molecular dimer ( $\sim 10^{-7} \mu\text{g m}^{-3}$ ) is significantly lower than that of most of the bulk IEPOX-SOA (Fig. 1d). This suggests that IEPOX-SOA may exist as oligomers in the aerosol phase, but that the oligomers were not evaporating as oligomers, rather decomposing and evaporating as monomer species at temperatures intermediate with those corresponding to the  $C^*$  of the monomers and the dimers, consistent with results of Lopez-Hilfiker et al. (2016). Although the IEPOX organosulfate may have lower volatility than estimated in Fig. 1d, it only accounts for 24 % of total IEPOX-SOA (Hu et al., 2015), and thus it cannot be the only reason for the low volatility of the bulk of IEPOX-SOA. For reference, only 5 % of the total sulfate is due to the IEPOX organosulfate, with the rest being inorganic sulfate consistent with other results from the SE US in summer 2013 (Liao et al., 2015). Indeed, the thermogram of total sulfate is very different from that of IEPOX-SOA (Figs. 1a and 2a).

Further evidence supporting low volatility and strong oligomerization of IEPOX-SOA molecular species has also been reported. Lin et al. (2014) showed oligomers as part of IEPOX-SOA in filter-based LC/MS measurement at three sites (including CTR) during the SE US study. Some of the oligomers were separated by mass units of 100 ( $\text{C}_5\text{H}_8\text{O}_2$ ) and 82 ( $\text{C}_5\text{H}_6\text{O}$ ), which would be consistent with  $\text{C}_5$ -alkene triol ( $\text{C}_5\text{H}_{10}\text{O}_3$ ) and methyltetrol ( $\text{C}_5\text{H}_{12}\text{O}_4$ ) oligomerization through dehydration reactions ( $-\text{H}_2\text{O}$  or  $2 \text{H}_2\text{O}$ ), or with other reactions resulting in similar products. Results from online gas-particle partitioning measurements at the same site during this study have shown that the measured particle-phase fractions ( $F_p$  negatively correlated with  $C^*$ ) of ambient IEPOX-SOA tracers (e.g., 2-methyltetrols and  $\text{C}_5$ -alkene triols) are much higher than expected based on the species vapor pressures, consistent with these tracers being formed during GC analysis by decomposition of larger molecules (likely oligomers) (Isaacman-VanWertz et al., 2016). Thus, the low volatility of IEPOX-SOA estimated from our TD data is consistent with multiple other measurements.

It is of high interest to estimate the fractional losses for both OA and IEPOX-SOA due to isothermal evaporation upon dilution. These losses can be estimated using the volatility distributions estimated from the TD measurements. This parameter can be quantified as (Cappa and Jimenez, 2010)

$$E_{\text{loss}} = 100\% \left[ 1 - \frac{C_{\text{OA}}(\text{DF})}{C_{\text{OA}}(0)/\text{DF}} \right], \quad (1)$$

where  $E_{\text{loss}}$  is the fractional OA loss due to evaporation,  $C_{\text{OA}}(0)$  is the initial organic mass concentration before dilution, and DF is the dilution factor applied.  $C_{\text{OA}}(\text{DF})$  is the OA concentration in equilibrium after dilution. Dilution factors varying from 1 to 30 were used here. The results are shown in Fig. 1c. After a 30-fold dilution, IEPOX-SOA mass loss due to evaporation is estimated to be  $\sim 5\%$ , substantially lower than for total OA (17 %). There are two uncertainties affecting this result. One is that the real volatility distribution of IEPOX-SOA is likely even lower, since the TD results are thought to be affected by oligomer decomposition upon heating. The other one is that this calculation neglects the effect of possible decomposition of oligomers into monomers in ambient air. If that process occurs on a timescale of, e.g., 1 day, it would lead to higher evaporated fractions than estimated here. The residence time of TD is  $\sim 10\text{--}15$  s, which may not be sufficient time for oligomer decomposition, especially at the lower temperatures that determined the upper end of the estimated volatility distribution. For example, Vaden et al. (2011) reported that it took 24 h to evaporate 75 % of  $\alpha$ -pinene SOA (although it is possible that processes other than oligomer decomposition were important for determining the timescale of those experiments). The kinetics of oligomer decomposition of IEPOX-SOA under ambient conditions should be further investigated to fully constrain its evaporation dynamics.

### 3.2 Fate of gas-phase IEPOX

IEPOX-SOA loadings exhibited a continuous decrease as OH exposure increases in the OFR. To interpret the observed decay of IEPOX-SOA in the OFR, we first need to understand whether additional IEPOX-SOA was formed in the OFR during the SE US study. More details about the IEPOX-SOA decay will be discussed in Sect. 3.3. Here, the box model described above (Fig. 3) was used to simulate the fate of gas-phase IEPOX in OFR and ambient conditions, as shown in Fig. 4.

In ambient air, gas-phase IEPOX will either react with OH radicals to form more oxidized gas-phase products (e.g., hydroxyacetone) (Bates et al., 2014, 2015), be taken up onto acidic aerosol (Surratt et al., 2010), or be lost from the atmosphere through dry or wet deposition (Nguyen et al., 2015). Photolysis of IEPOX in ambient air should be negligible, since the epoxide and hydroxyl groups in IEPOX are photostable at visible or actinic UV wavelengths (Fleming et al., 1959). A model scenario accounting for organic resistance with slower IEPOX uptake than pure inorganic is applied to simulate the fate of gas-phase IEPOX (Gaston et al., 2014; Riva et al., 2016). This scenario is the most realistic assumption, since 67 % of ambient aerosol is OA during the SE US study (Fig. S15). Results from an alternative model assuming pure inorganic aerosols are shown in the Supplement. The model predicts that the main pathway of gas-phase IEPOX removal in ambient air is aerosol-phase uptake during the

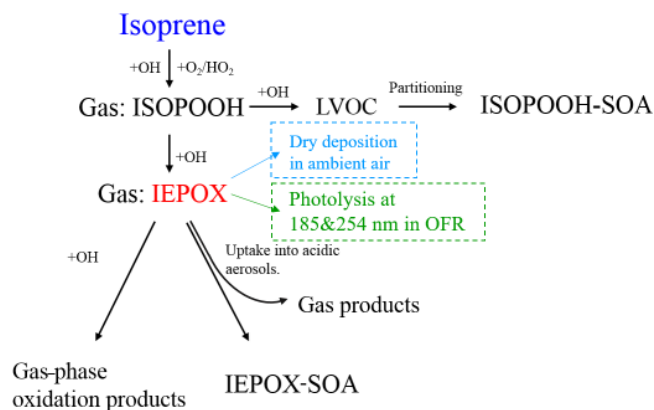


**Figure 3.** Mechanism diagram of gas-phase IEPOX model in ambient and OFR conditions. ISOPOOH-SOA refers to SOA formed through gas-particle partitioning of low-volatile VOCs from oxidation of isoprene 4-hydroxy-3-hydroperoxide (4,3-ISOPOOH) under low-NO conditions (Krechmer et al., 2015).

SE US study, where about 75 % of IEPOX was taken up by the aerosol after 1 day under ambient conditions, because of the efficient uptake of gas-phase IEPOX onto acidic ambient aerosols ( $\text{pH} = 0.8 \pm 0.5$ ) at the CTR site ( $\gamma_{\text{IEPOX}} = 0.009$ , lifetime  $\sim 1.8$  h). The rest of IEPOX was lost to dry deposition to the surface (16 %), according to reported boundary layer of 1200 m and dry deposition rate of  $3 \text{ cm s}^{-1}$  (Nguyen et al., 2015), or to gas-phase reaction with OH (9 %).

The fate of IEPOX sampled into the OFR differed from its fate in ambient air. Remaining unreacted and then leaving OFR or destruction in the gas phase completely dominate the fate of IEPOX under OFR conditions (Fig. 4b). Negligible amounts of IEPOX ( $< 1$  %) were taken up into the aerosol phase in the OFR. This is mainly because the lifetime of IEPOX aerosol uptake ( $\gamma_{\text{IEPOX}} = 0.002$ ; lifetime = 7.0 h) was much longer than the OFR residence time (200 s). The lower  $\gamma_{\text{IEPOX}}$  in OFR (0.002) than in the ambient condition (0.008) was because of the higher pH of aerosol leading to a slower IEPOX uptake. Higher pH in OFR ( $1.35 \pm 0.6$ ) than that in ambient ( $0.8 \pm 0.5$ ) was because extra neutralized inorganic aerosol was formed in OFR. Photolysis of IEPOX in OFR is estimated to be very minor (less than 0.2 %) (Fig. 4b and Table S3). Loss of IEPOX to the reactor walls is thought to be minor under the conditions of SE US study, given its high vapor pressure (Krechmer et al., 2015; Palm et al., 2016). We can estimate the timescale of IEPOX loss rate to the walls by assuming that the walls are covered by a layer of deposited ambient aerosol. We combine the first-order rate of collision of gas molecules with the walls (400 s; Palm et al., 2016) and the uptake coefficient for IEPOX-SOA in ambient aerosols ( $\gamma_{\text{IEPOX}} = 0.009$ ) to estimate a timescale of IEPOX loss to the walls of 12.3 h, which is negligible compared to the residence time of IEPOX ( $\sim 200$  s) in the OFR. Even if the walls were covered by sulfuric acid ( $\gamma_{\text{IEPOX}} = 0.082$ ), the timescale of loss would be 1.4 h.

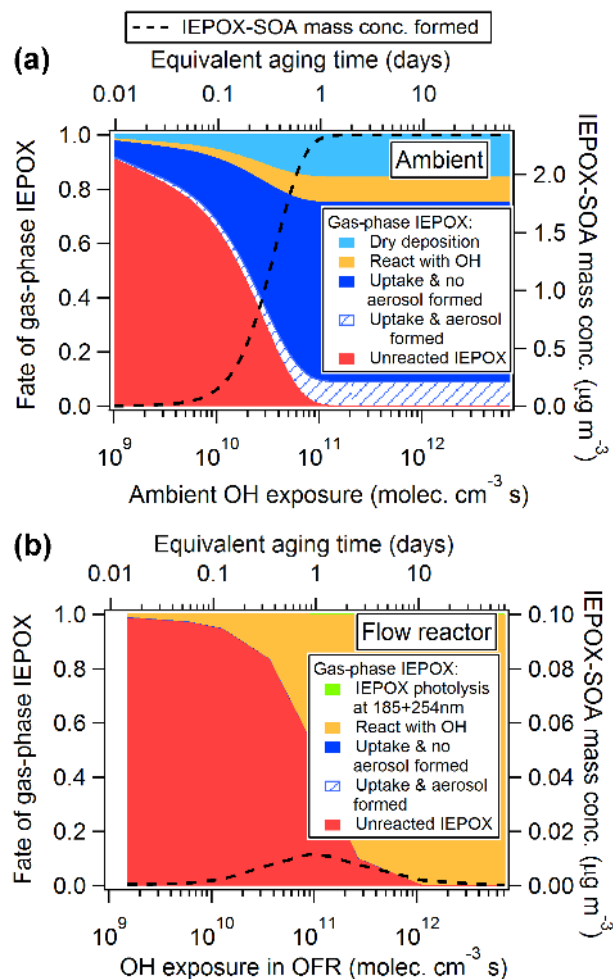


**Figure 4.** Modeled IEPOX fate (a) in ambient air and (b) oxidation flow reactor (OFR) conditions in the SE US study. The uptake rate of gas-phase IEPOX onto aerosol is calculated by using the model of Gaston et al. (2014), and is mainly influenced by aerosol pH (estimated as 0.8 and 1.35 for ambient and OFR aerosol, respectively) and aerosol surface areas ( $300$  and  $350 \mu\text{m}^2 \text{ cm}^{-3}$  for ambient and OFR aerosol, respectively). The calculated IEPOX-SOA mass concentrations are shown in the right axis of this figure. The OH exposures for both panels range  $15 \text{ min}^{-2}$  months of atmospheric equivalent age (at OH concentration =  $1.5 \times 10^6 \text{ molec cm}^{-3}$ ).

IEPOX-SOA mass concentrations formed in both ambient and OFR conditions were calculated as a function of OH exposure. For this estimate the molar mass of IEPOX-SOA and the SOA molar yield ( $\varphi_{\text{SOA}}$ ) of IEPOX, defined as the sum of formed aqueous-phase SOA tracer relative to the heterogeneous rate of gas-phase epoxide loss to particles (Riedel et al., 2015), are needed. Using the measured molecular composition of IEPOX-SOA (Hu et al., 2015), and assuming all species were present as dimers as discussed above, yields an average molar mass of bulk IEPOX-SOA of  $270 \text{ g mol}^{-1}$ . Laboratory uptake experiments showed that the SOA molar yield of IEPOX is around 10–12 %

for acidic  $(\text{NH}_4)_2\text{SO}_4$  (Riedel et al., 2015). A molar mass of  $270 \text{ g mol}^{-1}$  and  $\varphi_{\text{SOA}} = 6\%$  (to account for the dimerization) for IEPOX-SOA were applied here. In the OFR, the maximum modeled IEPOX-SOA mass concentrations were less than  $12 \text{ ng m}^{-3}$ , peaking at  $\sim 1$  day OH exposure. The model-predicted IEPOX-SOA formation is equivalent to  $\sim 1\%$  of the ambient IEPOX-SOA, indicating that negligible IEPOX-SOA was formed in the OFR. If the more detailed IEPOX-SOA formation model of Riedel et al. (2016) were used, the modeled IEPOX-SOA formation would be significantly lower, due to the consideration of the kinetics of IEPOX-SOA formation. That reinforces our conclusion that IEPOX-SOA formation in the reactor was negligible. An upper limit of  $\sim 6\%$  of the ambient IEPOX-SOA mass being formed in the OFR can be derived assuming that the particles are 100% inorganic, as shown in Fig. S16.

In addition to the box model results, we also have experimental evidence demonstrating negligible IEPOX-SOA formation in the OFR. During the Amazon study, standard additions of isoprene (50–200 ppb) were injected into ambient air at the entrance of the OFR, during a period when little SOA was formed from ambient precursors. After isoprene was exposed to varied OH exposures ( $\sim 10^9$ – $10^{12} \text{ molec cm}^{-3} \text{ s}$ ) in the OFR in the presence of ambient aerosols, no additional IEPOX-SOA formation was observed in the oxidized air exiting the OFR, as shown in Fig. 5. Even under optimum OH exposures ( $8$ – $11 \times 10^{10} \text{ molec cm}^{-3} \text{ s}$ ), where most of the isoprene and isoprene hydroxy hydroperoxide (ISOPOOH) are expected to be oxidized and before substantial decay of IEPOX-SOA occurs, no enhancements of IEPOX-SOA tracer  $\text{C}_5\text{H}_6\text{O}^+$  ion abundance in OA spectra were observed. Consistent with our results, a laboratory flow tube study (residence time of 1 min) of low-NO isoprene oxidation in the presence of acidified inorganic seeds also reported negligible IEPOX-SOA formation (Wong et al., 2015). Those results highlight a key limitation of this type of OFR: processes that do not scale with OH, and thus are not greatly accelerated in the reactor, are not captured. This limitation can be removed by seeding the OFR with  $\text{H}_2\text{SO}_4$  particles, which greatly accelerate IEPOX aerosol uptake. Simulation results (not shown) indicate that adding  $\sim 100 \mu\text{g m}^{-3}$  of pure  $\text{H}_2\text{SO}_4$  to the ambient air allows IEPOX-SOA to be efficiently formed in the reactor. The increased surface area and acidity from added  $\text{H}_2\text{SO}_4$  seed both help accelerate IEPOX reactive uptake, although acidity plays a more important role. If we use the ambient surface area and pure  $\text{H}_2\text{SO}_4$  in the model, the lifetime of IEPOX uptake is  $\sim 10$  min, while if we assume the ambient acidity and the same surface area as  $100 \mu\text{g m}^{-3}$  of pure  $\text{H}_2\text{SO}_4$ , the lifetime is 1.1 h.

### 3.3 Lifetime of IEPOX-SOA against OH oxidation

IEPOX-SOA loadings showed a continuous decrease as OH exposure increases in the OFR (Fig. 6a). Since negligible IEPOX-SOA mass was added in the OFR (Sect. 3.2), this

decay should be due to the sum of all IEPOX-SOA loss processes. The loss of IEPOX-SOA is defined empirically here as the loss of the molecular structures that result on AMS spectral features of IEPOX-SOA (e.g.,  $\text{C}_5\text{H}_6\text{O}^+$  and  $\text{C}_4\text{H}_5^+$  enhancements, Lin et al., 2012; Hu et al., 2015), such that an IEPOX-SOA component cannot be distinguished in constrained PMF analysis. Evaporation, photolysis and heterogeneous reaction with OH radicals are three possible loss pathways. Note that the rate derived here may be a lower limit for individual molecular components of IEPOX-SOA, if, e.g., it takes two or more OH reactions for their AMS spectrum to no longer resemble that of IEPOX-SOA.

In principle some IEPOX-SOA could evaporate if semivolatile molecules in equilibrium with it were oxidized by OH. As discussed above, IEPOX-SOA itself has low volatility, and only a small fraction ( $\sim 5\%$ ) may evaporate to the gas phase after dilution of a factor of 30. Oligomer decomposition followed by evaporation is very likely negligible in the flow reactor residence timescale of 3 min. However, this process could be more important in ambient air, and if fast, could influence the IEPOX-SOA lifetime. No results for oligomer decomposition rates or extents for IEPOX-SOA have been reported in the literature, to our knowledge. Thus, further research on this topic is recommended. Thus IEPOX-SOA evaporation is unlikely to contribute to the large observed IEPOX-SOA loss in the OFR (up to 90%).

Photolysis of IEPOX-SOA also cannot explain the large decreases of IEPOX-SOA in Fig. 6a. Washenfelder et al. (2015) reported that IEPOX-SOA during the SE US study contributed negligibly to the aerosol absorption at 365 nm. Lin et al. (2014) reported a wavelength-dependent effective mass absorption coefficient (MAC) value of  $\sim 247 \text{ cm}^2 \text{ g}^{-1}$  at 254 nm for laboratory-generated IEPOX-SOA on acidified  $(\text{NH}_4)_2\text{SO}_4$  seed. Using the MAC trend vs. wavelength and the measured data down to 200 nm we estimate an MAC of  $\sim 5200 \text{ cm}^2 \text{ g}^{-1}$  at 185 nm. Using those absorption efficiencies (and assuming an upper limit quantum yield of 1) we can derive an upper limit photolysis fraction of 1.5% of IEPOX-SOA in the OFR when neglecting other competing effects (e.g., OH oxidation, Table S3 and Fig. S17). In addition, the actual quantum yield may be much less than 1, as IEPOX-SOA molecular species contain mainly hydroxyl and carbonyl groups (Surratt et al., 2010; Lin et al., 2014). Interactions between these groups are thought to result in low quantum yields in the condensed phase (Phillips and Smith, 2014, 2015; Sharpless and Blough, 2014; Peng et al., 2016). Therefore, photolysis of IEPOX-SOA should contribute negligibly to the observed IEPOX-SOA decay.

The observed decay of IEPOX-SOA in Fig. 6a must then be the result of heterogeneous reactions with OH radicals.



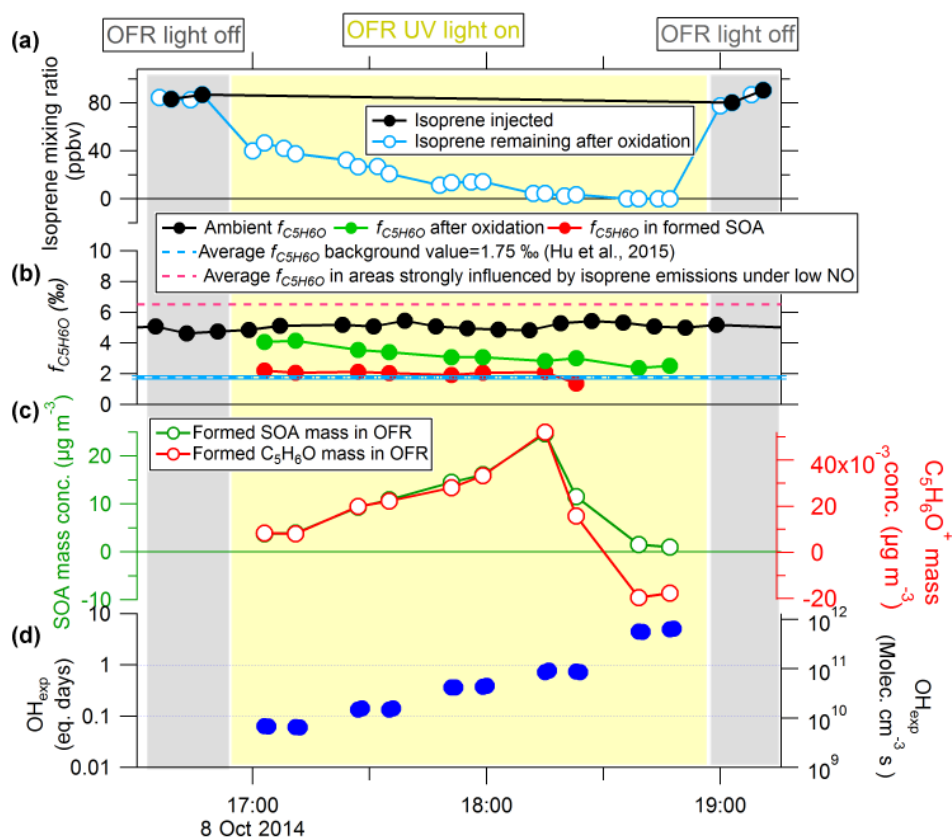


**Figure 5.** Isoprene standard addition experiment in ambient air during the GoAmazon2014/5 study. (a) Isoprene mass concentration injected and remaining after OFR. (b) Time series of ambient  $f_{C_5H_6O}$ ,  $f_{C_5H_6O}$  in OA after oxidation and  $f_{C_5H_6O}$  in newly formed SOA from OFR oxidation. The average background value  $f_{C_5H_6O} = 1.75\%$  from urban and biomass burning emissions and  $f_{C_5H_6O} = 6.5\%$  from aerosol strongly influenced by isoprene emissions are also shown (Hu et al., 2015). (c) Time series of mass concentration of newly formed SOA (left axis) and  $C_5H_6O^+$  (right axis). (d) Time series of equivalent aging time (left axis) and OH exposure in OFR (right axis). OH concentration =  $1.5 \times 10^6$  molec  $\text{cm}^{-3}$  was assumed here to calculate equivalent OH aging times. The gray background indicates OFR light off period and light yellow is OFR light on period. Different OH exposures were achieved by varying the UV light intensity. Residence time in the OFR was about 200 s.

This process can be quantitatively described as

$$\begin{aligned} [\text{IEPOX-SOA}]_i / [\text{IEPOX-SOA}]_0 &= e^{-k_{OH} \times OH_i \times \Delta t} \\ &= e^{-k_{OH} \times OH_i \times \Delta t} = e^{-k_{OH} \times OH_{exp, i}}, \end{aligned} \quad (2)$$

where  $[\text{IEPOX-SOA}]_i$  is the IEPOX-SOA mass concentration after the  $i$ th OH exposure step in the OFR.  $[\text{IEPOX-SOA}]_0$  is the initial ambient IEPOX-SOA entering the OFR;  $[\text{IEPOX-SOA}]_i / [\text{IEPOX-SOA}]_0$  is the mass fraction remaining of IEPOX-SOA in the OFR output, shown in Fig. 6a.  $OH_i$  is the average OH concentration of step  $i$  in the OFR;  $\Delta t$  is the real exposure time.  $OH_{exp, i} = OH_i \times \Delta t$  is the OH exposure of step  $i$ .  $k_{OH}$  is the heterogeneous reaction rate coefficient between IEPOX-SOA and OH radicals.

Fitting the results in Fig. 6a with Eq. (2) results in a  $k_{OH}$  of  $4.0 \pm 2.0 \times 10^{-13}$   $\text{cm}^3 \text{molec}^{-1} \text{s}^{-1}$ . The  $1\sigma$  uncertainty was obtained by Monte Carlo simulation, from propagation of the errors of  $[\text{IEPOX-SOA}]_i / [\text{IEPOX-SOA}]_0$  (9%) and the uncertainty of OH exposure (35%, Fig. S4). The uncertainty of

$[\text{IEPOX-SOA}]_i / [\text{IEPOX-SOA}]_0$  was estimated as 9% from PMF analysis of OFR data (Hu et al., 2015).

A similar  $k_{OH}$  value ( $4.6 \times 10^{-13}$   $\text{cm}^3 \text{molec}^{-1} \text{s}^{-1}$ ) was obtained by fitting the IEPOX-SOA tracer  $C_5H_6O^+$  ion decay as a function of OH exposure during a period (26 June, 14:00–19:00) when 80–90% of ambient OA was composed of IEPOX-SOA (Figs. S18–S19), which confirms the  $k_{OH}$  determined above.

For comparison, the average mass fraction remaining of IEPOX-SOA vs. OH exposure during the Amazon study is also shown in Fig. 6a. A similar  $k_{OH}$  value of  $3.9 \pm 1.8 \times 10^{-13}$   $\text{cm}^3 \text{molec}^{-1} \text{s}^{-1}$  was obtained. Despite differences between the SE and Amazon studies, the similarity of results from both studies increases our confidence in the derived value of the heterogeneous reaction rate coefficient. The higher aerosol concentrations from biomass burning during the Amazon study did not appear to cause any major differences in the observed OH uptake. This may be due to the mostly liquid state of the ambient particles in both

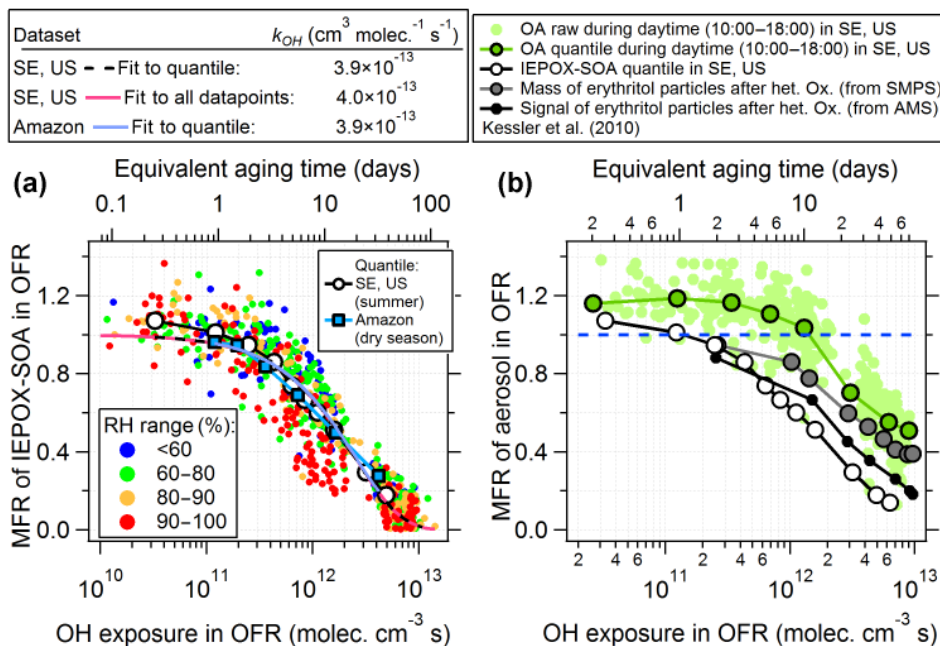


**Figure 6.** (a) Mass fraction remaining (MFR) of IEPOX-SOA in OFR output as a function of OH exposure during the entire SE US study and GoAmazon 2014/5 (dry season) studies. Individual datapoints from the SE US study are color-coded by ambient RH. Similar data for GoAmazon 2014/5 are shown in Fig. S21. (b) Mass fraction of OA remaining in OFR output as a function of OH exposure in daytime (12:00–18:00) during the SE US study. Also shown is the MFR of pure erythritol particles after heterogeneous oxidation as detected by SMPS and by AMS for reference (Kessler et al., 2010). Erythritol has a similar structure to the IEPOX-SOA tracers 2-methyltetrols.

studies (Bateman et al., 2016; Pajunoja et al., 2016), which will be discussed in detail below.

To investigate  $k_{OH}$  of OA, multiple experiments (usually with  $\text{RH} < 30\%$ ) with laboratory-generated different types of OA have been conducted. The bulk of those OA in the lab usually had mobility particle sizes ranging from 100 to 300 nm (Table 1), similar to that of IEPOX-SOA in SE US (wet size = 415 nm). The  $k_{OH}$  value of IEPOX-SOA determined here is similar to heterogeneous  $k_{OH}$  determined in those laboratory studies, including highly oxidized OA (e.g., citric acid;  $3.3\text{--}7.6 \times 10^{-13} \text{ cm}^3 \text{ molec.}^{-1} \text{ s}^{-1}$ ) (Kessler et al., 2012), levoglucosan ( $1.4\text{--}4.3 \times 10^{-13} \text{ cm}^3 \text{ molec.}^{-1} \text{ s}^{-1}$ ) (Slade and Knopf, 2014), and pure erythritol ( $2.5 \times 10^{-13} \text{ cm}^3 \text{ molec.}^{-1} \text{ s}^{-1}$ ), which has a similar structure to the 2-methyltetrols in IEPOX-SOA (Kessler et al., 2010). A summary of  $k_{OH}$  in this study and other laboratory studies with additional experimental information for each study is shown in Table 1.

A dependence of  $k_{OH}$  on ambient RH was found in both the SE US and Amazon studies, with larger  $k_{OH}$  at high RH, especially above 90% RH (Fig. 7). This effect may be due to higher liquid water content, leading to a larger surface area that facilitates faster OH uptake to the aerosol phase, and thus resulting in faster  $k_{OH}$  values. Accounting for liquid water content, the calculated particle surface areas show similar trends to  $k_{OH}$  in both studies, as shown in Fig. 7. The

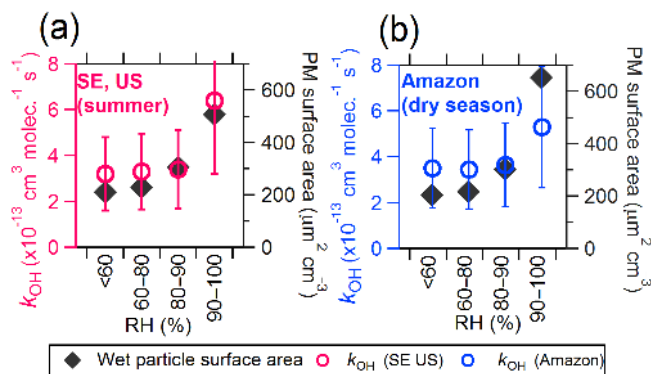


**Figure 7.** Estimated  $k_{OH}$  of IEPOX-SOA vs. ambient RH during the SE US and Amazon studies. The ambient wet particle surface areas in both studies are shown on the right axis.

values of both parameters increase with RH (especially for  $\text{RH} > 90\%$ ).

An alternative explanation for the measured RH dependence would be the influence of diffusion limitations. However, at the RH levels studied here ( $> 40\%$ ), diffusion limitations of OH in the aerosol phase are thought to be negligible (calculated lifetime of bulk diffusion of OH radical  $< 1 \text{ s}$ ). The diffusion coefficient of OH radical in liquid phase ( $> 10^{-14} \text{ m}^2 \text{ s}^{-1}$ ) was obtained from other laboratory-generated OA (e.g., isoprene-derived SOA,  $\alpha$ -pinene-derived

**Table 1.** Summary of  $k_{\text{OH}}$ ,  $\gamma_{\text{OH}}$  and different experiment parameters used in this study and other lab studies.

Species Name	$k_{\text{OH}} \times 10^{12}$ ( $\text{cm}^3 \text{ molec}^{-1} \text{ s}^{-1}$ )	$\gamma_{\text{OH}}$	OH conc ( $\text{molec cm}^{-3}$ )	React. time	Particle size (nm)	RH	References
IEPOX-SOA in SE US	$0.40 \pm 0.20$	$0.59 \pm 0.33$	$10^7 - 10^{10}$	$\sim 200$ s	415	$\sim 83$ %	(1)
IEPOX-SOA	0.32	0.34	$10^7 - 10^{10}$	$\sim 200$ s	302	$< 60$ %	(1)
In SE US RH-dependent	0.33	0.39	$10^7 - 10^{10}$	$\sim 200$ s	328	60–80 %	(1)
	0.34	0.46	$10^7 - 10^{10}$	$\sim 200$ s	380	80–90 %	(1)
	0.64	1.19	$10^7 - 10^{10}$	$\sim 200$ s	525	90–100 %	(1)
IEPOX-SOA in Amazon	$0.39 \pm 0.19$	$0.68 \pm 0.38$	$10^7 - 10^{10}$	$\sim 200$ s	490	$\sim 86$ %	(1)
IEPOX-SOA in	0.35	0.45	$10^7 - 10^{10}$	$\sim 200$ s	363	$< 60$ %	(1)
Amazon RH-	0.35	0.46	$10^7 - 10^{10}$	$\sim 200$ s	380	60–80 %	(1)
dependent	0.37	0.54	$10^7 - 10^{10}$	$\sim 200$ s	415	80–90 %	(1)
	0.53	1.09	$10^7 - 10^{10}$	$\sim 200$ s	576	90–100 %	(1)
Highly oxidized organic species							
BTA <sup>a</sup>	0.76	0.51	$\sim 10^9 - 3 \times 10^{11}$	$\sim 37$ s	$\sim 130 - 145$	30 %	(2)
Citric acid	0.43	0.37	$\sim 10^9 - 3 \times 10^{11}$	$\sim 37$ s	$\sim 130 - 145$	30 %	(2)
Tartaric acid	0.33	0.40	$\sim 10^9 - 3 \times 10^{11}$	$\sim 37$ s	$\sim 130 - 145$	30 %	(2)
Erythritol	0.25	0.77	$\sim 1 \times 10^9 - 2 \times 10^{11}$	$\sim 37$ s	$\sim 200$	30 %	(3)
Motor oil particles							
Diesel particles	0.4–34	0.1–8	$0.6 - 40 \times 10^6$	4 h	$\sim 300$	10–75 %	(4)
Nucleated motor oil particles	NA	0.72	$0 - 3 \times 10^{10}$	37 s	$\sim 170$	$\sim 30$ %	(5)
Biomass burning tracers							
Levoglucosan	0.31	0.91	$\sim 1 \times 10^9 - 2 \times 10^{11}$	$\sim 37$ s	$\sim 200$	30 %	(3)
	0.14–0.43	0.21–0.65	$10^8$ to $10^9$	NA	120–267	0–40 %	(6)
	NA	0.15–0.6	$10^7 - 10^{11}$	$< 1$ s	NA	0 %	(7)
Abietic acid	NA	0.15–0.6	$10^7 - 10^{11}$	NA	NA	0 %	(7)
Nitroguaiacol	NA	0.2–0.5	$10^7 - 10^{11}$	NA	NA	0 %	(7)
MNC <sup>b</sup>	0.04–0.16	0.07–0.22	$10^8$ to $10^9$	NA	203–307	0–26 %	(6)
Other pure organic species							
Squalene	NA	$0.3 \pm 0.07$	$1 \times 10^{10}$	$\sim 37$ s	$\sim 160$	30 %	(8)
Squalene	1.8–1.9	0.49–0.54	$1 - 7 \times 10^8$	1.5–3 h	$\sim 220$	30 %	(9)
Palmitic acid	NA	0.8–1	$1.4 - 3 \times 10^{10}$	10–17 s	85–220	$\sim 16$ %	(10)

<sup>a</sup> 1, 2, 3, 4-Butanetetra-carboxylic acid. <sup>b</sup> 4-methyl-5-Nitrocatechol. (1) This study. (2) Kessler et al. (2012). (3) Kessler et al. (2010). (4) Weitkamp et al. (2008). (5) Isaacman et al. (2012). (6) Slade and Knopf (2014). (7) Slade and Knopf (2013). (8) Smith et al. (2009). (9) Che et al. (2009). (10) McNeill et al. (2008). NA = not available

SOA, levoglucosan particles) (Renbaum-Wolff et al., 2013; Arangio et al., 2015; Y. J. Li et al., 2015; Song et al., 2015). Y. J. Li et al. (2015) reported that the diffusion of  $\text{NH}_3$  on laboratory biogenic SOA is only slowed at much lower transition RH (10–40 %) than that for liquid/solid-phase transition (50–80 %). This supports that under the conditions in SE US and Amazon studies, diffusion limitations should not play a role. An effect of temperature on  $k_{\text{OH}}$  was not apparent in our study. Lai et al. (2015) reported a significant effect for a laboratory study with a pure compound. We recommend that this issue is explored further in the laboratory using pure IEPOX-SOA.

The ambient lifetime of IEPOX-SOA due to the heterogeneous reaction with OH radicals was estimated to be more than 2 weeks ( $19 \pm 9$  days) based on the average  $k_{\text{OH}}$  ( $4.0 \pm 2.0 \times 10^{-13} \text{ cm}^3 \text{ molec}^{-1} \text{ s}^{-1}$ ), assuming an average ambient OH concentration of  $1.5 \times 10^6 \text{ molec cm}^{-3}$ . A similar lifetime can be estimated for the Amazon study. Longer lifetimes of 48 days in the SE US

study and 99 days in the Amazon study were estimated when the observed average 24 h OH concentrations in both studies ( $0.6 \times 10^6 \text{ molecule cm}^{-3}$  in SE US and  $0.3 \times 10^6 \text{ molecule cm}^{-3}$  in Amazon) were used (Krechmer et al., 2015). The long lifetime of IEPOX-SOA against heterogeneous oxidation is consistent with the estimated lifetime of total OA in urban and forested areas (Ortega et al., 2016; Palm et al., 2016), and also pure highly oxidized OA (1–2 weeks) in laboratory studies (Kessler et al., 2010, 2012).

### 3.4 Fate of oxidized IEPOX-SOA mass

It is of interest to determine whether the mass of IEPOX-SOA continues to be present in the aerosol after OH heterogeneous oxidation, albeit as a different chemical form, or whether it evaporates from the particles. Functionalization reactions would favor the former, while fragmentation reactions would favor the latter (George et al., 2007).

At lower OH exposures ( $< 1 \times 10^{12}$  molec  $\text{cm}^{-3}$  s) during daytime, SOA formation (non-IEPOX-SOA) was observed in the OFR (e.g., from monoterpene and sesquiterpenes oxidation, Fig. 6b), making it difficult to discern whether functionalization or fragmentation dominated for IEPOX-SOA losses. However, at OH exposures in the OFR above  $1 \times 10^{12}$  molec  $\text{cm}^{-3}$  s, net SOA formation from ambient air was no longer observed. This is presumably due to organic vapors undergoing multiple generations of oxidation and fragmenting in the gas phase in the OFR (Palm et al., 2016). For that OH exposure range, changes of the aerosol phase should be dominated by heterogeneous reactions. In this regime, OA mass was lost at a rapid rate of  $\sim 6\%$  OA mass per  $1 \times 10^{12}$  molec  $\text{cm}^{-3}$  s of OH exposure through volatilization. A very similar rate was observed for the IEPOX-SOA ( $\sim 7\%$  per  $1 \times 10^{12}$  molec  $\text{cm}^{-3}$  s), which implies that the main loss mechanism of IEPOX-SOA at higher OH exposures is due to volatilization following fragmentation. In the period when 80–90% of OA was composed of IEPOX-SOA, the OA also showed an up to 70% mass loss (Fig. S19), confirming the conclusion that a high fraction of IEPOX-SOA was volatilized to the gas phase after heterogeneous reaction at higher OH exposures.

The aerosol mass losses of IEPOX-SOA and OA into the gas phase are consistent with laboratory experiments of the heterogeneous reaction of pure erythritol particles (a surrogate of the IEPOX-SOA tracer 2-methyltetrols; see Fig. 6b), which also showed that OH oxidation led to the formation of volatile products escaping to the gas phase (Kessler et al., 2010; Kroll et al., 2015). We note, however, that IEPOX-SOA is mostly composed of oligomers rather than monomers, as with erythritol.

### 3.5 Estimation of reactive uptake coefficient ( $\gamma$ ) of OH

By quantifying the removal of IEPOX-SOA in the aerosol phase, an effective reactive uptake coefficient of OH ( $\gamma_{\text{OH}}$ ) on the aerosol in the OFR can be estimated. To our knowledge, this is the first time that  $\gamma_{\text{OH}}$  has been derived from measurements of ambient SOA aging.

The variable  $\gamma_{\text{OH}}$  can be calculated from  $k_{\text{OH}}$  per Smith et al. (2009):

$$\begin{aligned} \gamma_{\text{OH}} &= \frac{4 \cdot k_{\text{OH}} \cdot V_{\text{IEPOX-SOA}} \cdot \rho_0 \cdot N_{\text{A}}}{\bar{c} \cdot S_{\text{IEPOX-SOA}} \cdot \text{MW}_{\text{IEPOX-SOA}}} \\ &= \frac{4 \cdot k_{\text{OH}} \cdot D_{\text{surf}} \cdot \rho_0 \cdot N_{\text{A}}}{\bar{c} \cdot \text{MW}_{\text{IEPOX-SOA}}}, \end{aligned} \quad (3)$$

where  $k_{\text{OH}}$  is the heterogeneous reaction rate coefficient of IEPOX-SOA discussed above ( $4.2 \pm 2.1 \times 10^{-13}$   $\text{cm}^3$  molec $^{-1}$  s $^{-1}$ );  $\rho_0$  is density of aerosol in OFR, which is estimated as  $1.46 \pm 0.49$  g  $\text{cm}^{-3}$  based on the aerosol composition (Fig. S15).  $N_{\text{A}}$  is Avogadro's number;  $\bar{c}$  is the mean speed of gas-phase OH radicals, calculated as  $(8RT/\pi M)^{0.5}$ . ( $R$  is the universal gas constant,  $T$  is the temperature in K, and  $M$  is the molar mass

of the OH radical.) The calculated  $\bar{c}$  for OH (at 293 K) is  $604$  m s $^{-1}$ .  $\text{MW}_{\text{IEPOX-SOA}}$  is the molar mass of IEPOX-SOA. The estimated  $\text{MW}_{\text{IEPOX-SOA}} = 270$  g mol $^{-1}$  was used here, which is similar to isoprene-SOA molar mass of  $252$  g mol $^{-1}$  estimated from a separate flow tube study based on cloud condensation nuclei (CCN) measurement (King et al., 2010). An uncertainty of 30% is assigned to  $\text{MW}_{\text{IEPOX-SOA}}$ .  $V_{\text{IEPOX-SOA}}$  and  $S_{\text{IEPOX-SOA}}$  are the mean volume and surface areas of IEPOX-SOA. We assume IEPOX-SOA is uniformly mixed with the other aerosol species (both in the surface and volume), and is independent of particle size. Then for a spherical particle,  $V_{\text{total}}/S_{\text{total}}$  is equal to  $d_{\text{surf}}/6$ , where  $d_{\text{surf}}$  is defined as surface-weighted particle diameter. The dried surface-weighted aerodynamic size distribution of  $m/z$  82 (background corrected), tracer of IEPOX-SOA (Hu et al., 2015), peaks around 400 nm (Fig. 8), which is equivalent to a mobility size of  $\sim 274$  nm. By applying the average particle size growth factor of 1.5 calculated from average kappa (0.27) and ambient RH (T. K. V. Nguyen et al., 2014), the average  $d_{\text{surf}}$  of wet IEPOX-SOA is estimated as 410 nm. A similar method was applied to calculate  $d_{\text{surf}}$  of wet IEPOX-SOA in the Amazon study, which is finally calculated to be 490 nm.

The average mass-weighted aerodynamic size distribution of  $m/z$  82 in the SE US and Amazon studies ( $d_{\text{va}} = \sim 500$  and 600 nm) is consistent with that of sulfate ( $d_{\text{va}} = \sim 450$  and 510 nm), which may indicate sulfate control of the IEPOX uptake formation pathway (Xu et al., 2014; Liao et al., 2015; Marais et al., 2016). Both peaks of  $m/z$  82 and sulfate were systematically larger than of total OA ( $d_{\text{va}} = \sim 370$  or 400 nm), suggesting the IEPOX-SOA formation in SE US and Amazon studies may be partially contributed by aqueous/cloud processing (Meng and Seinfeld, 1994). The systematically higher oxidation level of IEPOX-SOA in the ambient air than from chamber studies also supports this conclusion (Chen et al., 2015; Hu et al., 2015).

Finally,  $\gamma_{\text{OH}}$  is estimated as  $0.59 \pm 0.33$  under a range of OH concentrations between  $5 \times 10^7$  and  $5 \times 10^{10}$  molec  $\text{cm}^{-3}$ , which is consistent with the range of  $\gamma_{\text{OH}}$  (0.37–0.77) calculated for highly oxidized OA in laboratory studies (Table 1). The uncertainty of  $\gamma_{\text{OH}}$  was estimated by Monte Carlo simulation, propagated from errors of each parameter in Eq. (2) (50% for  $k_{\text{OH}}$ , 30% for  $d_{\text{surf}}$ , 28% for  $\rho_0$ , and 30% for  $\text{MW}_{\text{IEPOX-SOA}}$ ). When considering the apparent RH effect on  $k_{\text{OH}}$ , the estimated  $\gamma_{\text{OH}}$  varies between 0.34 and 1.19. The  $\gamma_{\text{OH}}$  above 1 at the highest RH range (90–100%) might be due to secondary reactions of IEPOX-SOA in the more dilute liquid phase. The estimated  $\gamma_{\text{OH}}$  in the Amazon study is around  $0.68 \pm 0.38$ .

Ambient particles in both the SE US and GoAmazon studies were liquid as quantified by particle bounce experiments (Bateman et al., 2015; Pajunoja et al., 2016), and thus kinetic limitations to OH uptake in the OFR should not play a role (Y. J. Li et al., 2015). In this study, we calculated  $\gamma_{\text{OH}}$  based on a wide range of OH concentrations ( $5 \times 10^7$ –

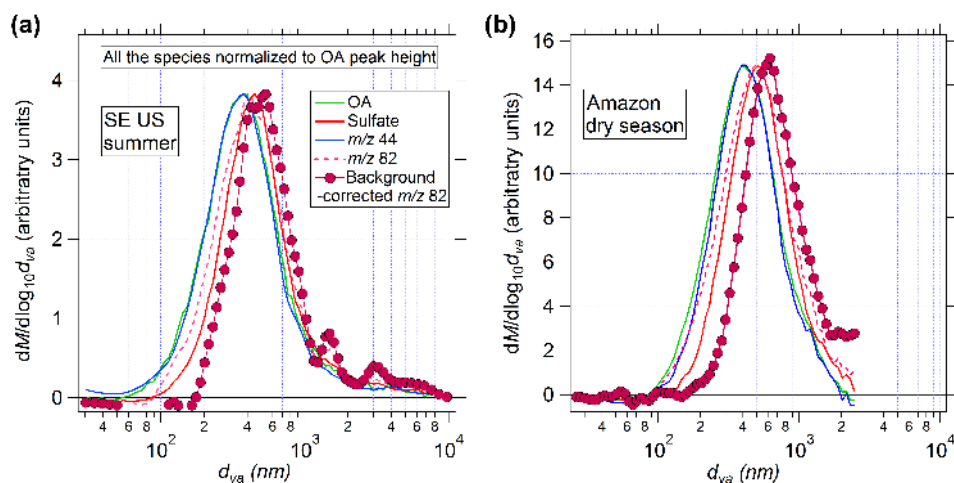


**Figure 8.** Average mass-weighted aerodynamic size distribution of OA, sulfate,  $m/z$  44, and  $m/z$  82 in (a) SE US and (b) Amazon. The mass size distribution of  $m/z$  82 with background correction is also shown. The background correction method was introduced in Hu et al. (2015). Heights of all the size distributions are set to the same value for ease of visual comparison.

$5 \times 10^{10}$  molec  $\text{cm}^{-3}$ ). Several laboratory experiments suggest that OH uptake should obey the Langmuir–Hinshelwood (LH) kinetic mechanism, where  $\gamma_{\text{OH}}$  tends to lower under higher OH concentrations, because of a saturation of surface reactive sites at higher OH concentrations (George and Abbatt, 2010; Slade and Knopf, 2013). We have calculated  $k_{\text{OH}}$  at different OH exposure ranges ( $10^{10}$  to  $10^{11}$ – $10^{13}$  molec  $\text{cm}^{-3}$   $\text{s}^{-1}$ , Fig. S22). No obvious OH dependence of  $k_{\text{OH}}$  ( $\gamma_{\text{OH}}$ ) was found above  $3 \times 10^9$  molec  $\text{cm}^{-3}$  (beyond where  $k_{\text{OH}}$  calculation is more robust), which suggests the  $\gamma_{\text{OH}}$  calculated in this study does not depend on OH concentration. A possible explanation is that in our study, OH uptake occurs on liquid particles, resulting on fast OH diffusion into the particle bulk, and causing OH uptake not to be limited by surface adsorption. We note that our experiments do not rule out some dependence of  $\gamma_{\text{OH}}$  on OH at lower OH levels in the atmosphere. However, Che et al. (2009) found no effect of OH on  $\gamma_{\text{OH}}$  for squalane particles in the range  $1$ – $7 \times 10^8$  molec  $\text{cm}^{-3}$ . More consideration of other factors (e.g., surface regeneration due to volatilization; aerosol-phase influence) should be explored in future studies of the  $\gamma_{\text{OH}}$  for IEPOX-SOA.

#### 4 Conclusions

We investigated volatility and aging processes of IEPOX-SOA during the late spring and early summer of SE US and the dry season of central Amazonia with a field-deployed thermodenuder and an oxidation flow reactor. IEPOX-SOA had a volatility distribution much lower than those of the monomer tracers that have been reported as comprising most of its mass. Much of IEPOX-SOA likely exists as oligomers in the aerosol phase. The kinetics of decomposi-

tion of oligomers to monomers needs further investigation to fully constrain the lifetime of IEPOX-SOA against evaporation.

The formation of IEPOX-SOA in the field and in the OFR flow reactor was investigated. In contrast to the efficient IEPOX uptake in the ambient air, negligible IEPOX-SOA was formed in the OFR under OH oxidation, as the OFR as used here does not accelerate processes such as aerosol uptake and reactions that do not scale with OH. Simulation results indicate that adding  $\sim 100 \mu\text{g m}^{-3}$  of pure  $\text{H}_2\text{SO}_4$  to the ambient air would allow IEPOX-SOA to be efficiently formed in the reactor. Photolysis and evaporation of IEPOX-SOA in the OFR contributed negligibly to IEPOX-SOA loss. From the OFR results, we determined that the lifetime of IEPOX-SOA through heterogeneous reaction with OH radicals ( $k_{\text{OH}} = 4.0 \pm 2.0 \times 10^{-13}$   $\text{cm}^3$  molecule $^{-1}$   $\text{s}^{-1}$  in the SE US study and  $3.9 \pm 1.8 \times 10^{-13}$   $\text{cm}^3$  molecule $^{-1}$   $\text{s}^{-1}$  in the Amazon study) is equivalent to more than a 2-week photochemical aging lifetime (assuming  $\text{OH} = 1.5 \times 10^6$  molec  $\text{cm}^{-3}$ ). The mass lost at high OH exposures is mainly volatilized, rather than transformed into other aerosol species with different composition, which suggests that fragmentation plays an important role during the ambient aging process.

Values of effective  $\gamma_{\text{OH}}$  based on the measured IEPOX-SOA  $k_{\text{OH}}$  and other particle parameters were determined to be  $0.59 \pm 0.33$  in SE US and  $0.68 \pm 0.38$  in Amazon with no dependence on OH concentration over the range  $5 \times 10^7$ – $5 \times 10^{10}$  molecule  $\text{cm}^{-3}$ . This is the first time that  $\gamma_{\text{OH}}$  was estimated based on ambient SOA. Positive correlation between  $\gamma_{\text{OH}}$  and wet particle surface areas (RH-dependent) suggest that OH uptake is surface-area-limited. The substantially larger size distribution of IEPOX-SOA tracer  $m/z$  82 and sulfate vs. bulk OA suggests that IEPOX-SOA formation



in the SE US study may be controlled by sulfate and/or influenced by cloud processing. However, the effect of aqueous processing under very dilute conditions relevant to clouds has not been investigated to our knowledge. Our results provide constraints on the sinks of IEPOX-SOA, which are useful for better quantifying OA impacts on air quality and climate.

## 5 Data availability

Part of the data used in this study is publicly available at: <http://esrl.noaa.gov/csd/groups/csd7/measurements/2013senex/Ground/DataDownload/>. Other data can be obtained from the authors upon request ([jose.jimenez@colorado.edu](mailto:jose.jimenez@colorado.edu)).

**The Supplement related to this article is available online at doi:10.5194/acp-16-11563-2016-supplement.**

*Acknowledgements.* This study was partially supported by EPRI-10004734, NSF AGS-1243354 and AGS-1360834, NASA NNX15AT96G, DOE (BER/ASR) DE-SC0011105, and NOAA NA13OAR4310063. Brett B. Palm and Jordan E. Krechmer were partially supported by EPA STAR fellowships (FP-91761701-0 & FP-91770901-0). We thank Annmarie Carlton, Eric Edgerton, and Karsten Baumann for their organization of the SE US supersite; Cassandra Gaston and Joel Thornton from the University of Washington for advice in the use of their IEPOX uptake model; Jian Wang from Brookhaven National Laboratory for advice on aerosol hygroscopicity during GoAmazon2014/5; Ying-Hsuan Lin and Jason D. Surratt from the University of North Carolina for sharing their published MAC data of IEPOX-SOA; Hongyu Guo and Rodney J. Weber from the Georgia Institute of Technology for providing their estimated pH for comparison to our pH calculation results; and John Crouse and Paul Wennberg from Caltech for gas-phase IEPOX and ISOPOOH data in the SE US study. This paper has not been reviewed by EPA and no endorsement should be inferred. A portion of the research was performed using EMSL, a DOE Office of Science User Facility sponsored by the Office of Biological and Environmental Research and located at Pacific Northwest National Laboratory. SEARCH network operations are supported by the Southern Company and EPRI.

Edited by: J. Allan

Reviewed by: two anonymous referees

## References

Allan, J. D., Morgan, W. T., Darbyshire, E., Flynn, M. J., Williams, P. I., Oram, D. E., Artaxo, P., Brito, J., Lee, J. D., and Coe, H.: Airborne observations of IEPOX-derived isoprene SOA in the Amazon during SAMBBA, *Atmos. Chem. Phys.*, 14, 11393–11407, doi:10.5194/acp-14-11393-2014, 2014.

- Arangio, A. M., Slade, J. H., Berkemeier, T., Pöschl, U., Knopf, D. A., and Shiraiwa, M.: Multiphase Chemical Kinetics of OH Radical Uptake by Molecular Organic Markers of Biomass Burning Aerosols: Humidity and Temperature Dependence, Surface Reaction, and Bulk Diffusion, *J. Phys. Chem. A*, 119, 4533–4544, doi:10.1021/jp510489z, 2015.
- Bateman, A. P., Gong, Z., Liu, P., Sato, B., Cirino, G., Zhang, Y., Artaxo, P., Bertram, A. K., Manzi, A. O., Rizzo, L. V., Souza, R. A. F., Zaveri, R. A., and Martin, S. T.: Sub-micrometre particulate matter is primarily in liquid form over Amazon rainforest, *Nat. Geosci.*, 9, 34–37, doi:10.1038/ngeo2599, 2016.
- Bates, K. H., Crouse, J. D., St. Clair, J. M., Bennett, N. B., Nguyen, T. B., Seinfeld, J. H., Stoltz, B. M., and Wennberg, P. O.: Gas Phase Production and Loss of Isoprene Epoxydiols, *J. Phys. Chem. A*, 118, 1237–1246, doi:10.1021/jp4107958, 2014.
- Bates, K. H., Nguyen, T. B., Teng, A. P., Crouse, J. D., Kjaergaard, H. G., Stoltz, B. M., Seinfeld, J. H., and Wennberg, P. O.: Production and Fate of C4 Dihydroxycarbonyl Compounds from Isoprene Oxidation, *J. Phys. Chem. A*, 120, 106–117, doi:10.1021/acs.jpca.5b10335, 2015.
- Budisulistiorini, S. H., Canagaratna, M. R., Croteau, P. L., Marth, W. J., Baumann, K., Edgerton, E. S., Shaw, S. L., Knipping, E. M., Worsnop, D. R., Jayne, J. T., Gold, A., and Surratt, J. D.: Real-Time Continuous Characterization of Secondary Organic Aerosol Derived from Isoprene Epoxydiols in Downtown Atlanta, Georgia, Using the Aerodyne Aerosol Chemical Speciation Monitor, *Environ. Sci. Technol.*, 47, 5686–5694, doi:10.1021/es400023n, 2013.
- Budisulistiorini, S. H., Li, X., Bairai, S. T., Renfro, J., Liu, Y., Liu, Y. J., McKinney, K. A., Martin, S. T., McNeill, V. F., Pye, H. O. T., Nenes, A., Neff, M. E., Stone, E. A., Mueller, S., Knote, C., Shaw, S. L., Zhang, Z., Gold, A., and Surratt, J. D.: Examining the effects of anthropogenic emissions on isoprene-derived secondary organic aerosol formation during the 2013 Southern Oxidant and Aerosol Study (SOAS) at the Look Rock, Tennessee ground site, *Atmos. Chem. Phys.*, 15, 8871–8888, doi:10.5194/acp-15-8871-2015, 2015.
- Canonaco, F., Crippa, M., Slowik, J. G., Baltensperger, U., and Prévôt, A. S. H.: SoFi, an IGOR-based interface for the efficient use of the generalized multilinear engine (ME-2) for the source apportionment: ME-2 application to aerosol mass spectrometer data, *Atmos. Meas. Tech.*, 6, 3649–3661, doi:10.5194/amt-6-3649-2013, 2013.
- Cappa, C. D. and Jimenez, J. L.: Quantitative estimates of the volatility of ambient organic aerosol, *Atmos. Chem. Phys.*, 10, 5409–5424, doi:10.5194/acp-10-5409-2010, 2010.
- Chattopadhyay, S. and Ziemann, P. J.: Vapor Pressures of Substituted and Unsubstituted Monocarboxylic and Dicarboxylic Acids Measured Using an Improved Thermal Desorption Particle Beam Mass Spectrometry Method, *Aerosol. Sci. Tech.*, 39, 1085–1100, doi:10.1080/02786820500421547, 2005.
- Che, D. L., Smith, J. D., Leone, S. R., Ahmed, M., and Wilson, K. R.: Quantifying the reactive uptake of OH by organic aerosols in a continuous flow stirred tank reactor, *Phys. Chem. Chem. Phys.*, 11, 7885–7895, doi:10.1039/b904418c, 2009.
- Chen, Q., Farmer, D. K., Rizzo, L. V., Pauliquevis, T., Kuwata, M., Karl, T. G., Guenther, A., Allan, J. D., Coe, H., Andreae, M. O., Pöschl, U., Jimenez, J. L., Artaxo, P., and Martin, S. T.: Submicron particle mass concentrations and sources in the Amazonian

- wet season (AMAZE-08), *Atmos. Chem. Phys.*, 15, 3687–3701, doi:10.5194/acp-15-3687-2015, 2015.
- DeCarlo, P. F., Kimmel, J. R., Trimborn, A., Northway, M. J., Jayne, J. T., Aiken, A. C., Gonin, M., Fuhrer, K., Horvath, T., Docherty, K. S., Worsnop, D. R., and Jimenez, J. L.: Field-deployable, high-resolution, time-of-flight aerosol mass spectrometer, *Anal. Chem.*, 78, 8281–8289, doi:10.1021/Ac061249n, 2006.
- Dzepina, K., Jimenez, J. L., Cappa, C. D., Volkamer, R. M., Madronich, S., DeCarlo, P. F., and Zaveri, R. A.: Modeling the Multiday Evolution and Aging of Secondary Organic Aerosol During MILAGRO 2006, *Environ. Sci. Technol.*, 45, 3496–3503, doi:10.1021/es103186f, 2011.
- Eddingsaas, N. C., VanderVelde, D. G., and Wennberg, P. O.: Kinetics and Products of the Acid-Catalyzed Ring-Opening of Atmospherically Relevant Butyl Epoxy Alcohols, *J. Phys. Chem. A*, 114, 8106–8113, doi:10.1021/jp103907c, 2010.
- Faulhaber, A. E., Thomas, B. M., Jimenez, J. L., Jayne, J. T., Worsnop, D. R., and Ziemann, P. J.: Characterization of a thermodenuder-particle beam mass spectrometer system for the study of organic aerosol volatility and composition, *Atmos. Meas. Tech.*, 2, 15–31, doi:10.5194/amt-2-15-2009, 2009.
- Fleming, G., Anderson, M. M., Harrison, A. J., and Pickett, L. W.: Effect of Ring Size on the Far Ultraviolet Absorption and Photolysis of Cyclic Ethers, *J. Phys. Chem. A*, 30, 351–354, doi:10.1063/1.1729951, 1959.
- Froyd, K. D., Murphy, S. M., Murphy, D. M., de Gouw, J. A., Eddingsaas, N. C., and Wennberg, P. O.: Contribution of isoprene-derived organosulfates to free tropospheric aerosol mass, *Proc. Natl. Acad. Sci. USA*, 107, 21360–21365, doi:10.1073/pnas.1012561107, 2010.
- Gaston, C. J., Riedel, T. P., Zhang, Z., Gold, A., Surratt, J. D., and Thornton, J. A.: Reactive Uptake of an Isoprene-Derived Epoxydiol to Submicron Aerosol Particles, *Environ. Sci. Technol.*, 48, 11178–11186, doi:10.1021/es5034266, 2014.
- George, C., Ammann, M., D’Anna, B., Donaldson, D. J., and Nizkorodov, S. A.: Heterogeneous Photochemistry in the Atmosphere, *Chem. Rev.*, 115, 4218–4258, doi:10.1021/cr500648z, 2015.
- George, I., Vlasenko, A., Slowik, J., and Abbatt, J.: Heterogeneous Oxidation of Saturated Organic Particles by OH, in: *Nucleation and Atmospheric Aerosols*, edited by: O’Dowd, C. and Wagner, P., Springer Netherlands, 736–740, 2007.
- George, I. J. and Abbatt, J. P. D.: Heterogeneous oxidation of atmospheric aerosol particles by gas-phase radicals, *Nature Chemistry*, 2, 713–722, 2010.
- Guenther, A. B., Jiang, X., Heald, C. L., Sakulyanontvittaya, T., Duhl, T., Emmons, L. K., and Wang, X.: The Model of Emissions of Gases and Aerosols from Nature version 2.1 (MEGAN2.1): an extended and updated framework for modeling biogenic emissions, *Geosci. Model Dev.*, 5, 1471–1492, doi:10.5194/gmd-5-1471-2012, 2012.
- Hallquist, M., Wenger, J. C., Baltensperger, U., Rudich, Y., Simpson, D., Claeys, M., Dommen, J., Donahue, N. M., George, C., Goldstein, A. H., Hamilton, J. F., Herrmann, H., Hoffmann, T., Iinuma, Y., Jang, M., Jenkin, M. E., Jimenez, J. L., Kiendler-Scharr, A., Maenhaut, W., McFiggans, G., Mentel, Th. F., Monod, A., Prévôt, A. S. H., Seinfeld, J. H., Surratt, J. D., Szmigielski, R., and Wildt, J.: The formation, properties and impact of secondary organic aerosol: current and emerging issues, *Atmos. Chem. Phys.*, 9, 5155–5236, doi:10.5194/acp-9-5155-2009, 2009.
- Hansen, D. A., Edgerton, E. S., Hartsell, B. E., Jansen, J. J., Kandasamy, N., Hidy, G. M., and Blanchard, C. L.: The Southeastern Aerosol Research and Characterization Study: Part 1 – Overview, *J. Air Waste Manage.*, 53, 1460–1471, doi:10.1080/10473289.2003.10466318, 2003.
- Hu, W. W., Campuzano-Jost, P., Palm, B. B., Day, D. A., Ortega, A. M., Hayes, P. L., Krechmer, J. E., Chen, Q., Kuwata, M., Liu, Y. J., de Sá, S. S., McKinney, K., Martin, S. T., Hu, M., Budisulistiorini, S. H., Riva, M., Surratt, J. D., St. Clair, J. M., Isaacman-Van Wertz, G., Yee, L. D., Goldstein, A. H., Carbone, S., Brito, J., Artaxo, P., de Gouw, J. A., Koss, A., Wisthaler, A., Mikoviny, T., Karl, T., Kaser, L., Jud, W., Hansel, A., Docherty, K. S., Alexander, M. L., Robinson, N. H., Coe, H., Allan, J. D., Canagaratna, M. R., Paulot, F., and Jimenez, J. L.: Characterization of a real-time tracer for isoprene epoxydiols-derived secondary organic aerosol (IEPOX-SOA) from aerosol mass spectrometer measurements, *Atmos. Chem. Phys.*, 15, 11807–11833, doi:10.5194/acp-15-11807-2015, 2015.
- Huffman, J. A., Docherty, K. S., Aiken, A. C., Cubison, M. J., Ulbrich, I. M., DeCarlo, P. F., Sueper, D., Jayne, J. T., Worsnop, D. R., Ziemann, P. J., and Jimenez, J. L.: Chemically-resolved aerosol volatility measurements from two megacity field studies, *Atmos. Chem. Phys.*, 9, 7161–7182, doi:10.5194/acp-9-7161-2009, 2009a.
- Huffman, J. A., Ziemann, P. J., Jayne, J. T., Worsnop, D. R., and Jimenez, J. L.: Development and Characterization of a Fast-Stepping/Scanning Thermodenuder for Chemically-Resolved Aerosol Volatility Measurements (vol 42, pg 395, 2008), *Aerosol Sci. Tech.*, 43, 273–273, doi:10.1080/02786820802616885, 2009b.
- Isaacman, G., Chan, A. W. H., Nah, T., Worton, D. R., Ruehl, C. R., Wilson, K. R., and Goldstein, A. H.: Heterogeneous OH Oxidation of Motor Oil Particles Causes Selective Depletion of Branched and Less Cyclic Hydrocarbons, *Environ. Sci. Technol.*, 46, 10632–10640, doi:10.1021/es302768a, 2012.
- Isaacman-VanWertz, G., Yee, L. D., Kreisberg, N. M., Wernis, R., Moss, J. A., Hering, S. V., de Sa, S. S., Martin, S. T., Alexander, L. M., Palm, B. B., Hu, W., Campuzano-Jost, P., Day, D. A., Jimenez, J. L., Riva, M., Surratt, J. D., Viegas, J., Manzi, A., Edgerton, E. S., Baumann, K., Souza, R., Artaxo, P., and Goldstein, A. H.: Ambient gas-particle partitioning of tracers for biogenic oxidation, *Environ. Sci. Technol.*, doi:10.1021/acs.est.6b01674, 2016.
- Kanakidou, M., Seinfeld, J. H., Pandis, S. N., Barnes, I., Dentener, F. J., Facchini, M. C., Van Dingenen, R., Ervens, B., Nenes, A., Nielsen, C. J., Swietlicki, E., Putaud, J. P., Balkanski, Y., Fuzzi, S., Horth, J., Moortgat, G. K., Winterhalter, R., Myhre, C. E. L., Tsigaridis, K., Vignati, E., Stephanou, E. G., and Wilson, J.: Organic aerosol and global climate modelling: a review, *Atmos. Chem. Phys.*, 5, 1053–1123, doi:10.5194/acp-5-1053-2005, 2005.
- Kang, E., Root, M. J., Toohey, D. W., and Brune, W. H.: Introducing the concept of Potential Aerosol Mass (PAM), *Atmos. Chem. Phys.*, 7, 5727–5744, doi:10.5194/acp-7-5727-2007, 2007.
- Karl, T., Guenther, A., Yokelson, R. J., Greenberg, J., Potosnak, M., Blake, D. R., and Artaxo, P.: The tropical forest and fire emissions experiment: Emission, chemistry, and trans-

- port of biogenic volatile organic compounds in the lower atmosphere over Amazonia, *J. Geophys. Res.*, 112, D18302, doi:10.1029/2007jd008539, 2007.
- Kessler, S. H., Smith, J. D., Che, D. L., Worsnop, D. R., Wilson, K. R., and Kroll, J. H.: Chemical Sinks of Organic Aerosol: Kinetics and Products of the Heterogeneous Oxidation of Erythritol and Levoglucosan, *Environ. Sci. Technol.*, 44, 7005–7010, doi:10.1021/Es101465m, 2010.
- Kessler, S. H., Nah, T., Daumit, K. E., Smith, J. D., Leone, S. R., Kolb, C. E., Worsnop, D. R., Wilson, K. R., and Kroll, J. H.: OH-Initiated Heterogeneous Aging of Highly Oxidized Organic Aerosol, *J. Phys. Chem. A*, 116, 6358–6365, doi:10.1021/jp212131m, 2012.
- King, S. M., Rosenoern, T., Shilling, J. E., Chen, Q., Wang, Z., Biskos, G., McKinney, K. A., Pöschl, U., and Martin, S. T.: Cloud droplet activation of mixed organic-sulfate particles produced by the photooxidation of isoprene, *Atmos. Chem. Phys.*, 10, 3953–3964, doi:10.5194/acp-10-3953-2010, 2010.
- Krechmer, J. E., Coggon, M. M., Massoli, P., Nguyen, T. B., Crounse, J. D., Hu, W., Day, D. A., Tyndall, G. S., Henze, D. K., Rivera-Rios, J. C., Nowak, J. B., Kimmel, J. R., Mauldin, R. L., Stark, H., Jayne, J. T., Sipilä, M., Junninen, H., St. Clair, J. M., Zhang, X., Feiner, P. A., Zhang, L., Miller, D. O., Brune, W. H., Keutsch, F. N., Wennberg, P. O., Seinfeld, J. H., Worsnop, D. R., Jimenez, J. L., and Canagaratna, M. R.: Formation of Low Volatility Organic Compounds and Secondary Organic Aerosol from Isoprene Hydroxyhydroperoxide Low-NO Oxidation, *Environ. Sci. Technol.*, 49, 10330–10339, doi:10.1021/acs.est.5b02031, 2015.
- Kroll, J. H., Lim, C. Y., Kessler, S. H., and Wilson, K. R.: Heterogeneous Oxidation of Atmospheric Organic Aerosol: Kinetics of Changes to the Amount and Oxidation State of Particle-Phase Organic Carbon, *J. Phys. Chem. A*, 119, 10767–10783, doi:10.1021/acs.jpca.5b06946, 2015.
- Lai, C., Liu, Y., Ma, J., Ma, Q., and He, H.: Laboratory study on OH-initiated degradation kinetics of dehydroabietic acid, *Phys. Chem. Chem. Phys.*, 17, 10953–10962, doi:10.1039/c5cp00268k, 2015.
- Lambe, A. T., Ahern, A. T., Williams, L. R., Slowik, J. G., Wong, J. P. S., Abbatt, J. P. D., Brune, W. H., Ng, N. L., Wright, J. P., Croasdale, D. R., Worsnop, D. R., Davidovits, P., and Onasch, T. B.: Characterization of aerosol photooxidation flow reactors: heterogeneous oxidation, secondary organic aerosol formation and cloud condensation nuclei activity measurements, *Atmos. Meas. Tech.*, 4, 445–461, doi:10.5194/amt-4-445-2011, 2011.
- Li, R., Palm, B. B., Ortega, A. M., Hlywiak, J. A., Hu, W., Peng, Z., Day, D. A., Knote, C., Brune, W. H., de Gouw, J. A., and Jimenez, J. L.: Modeling the Radical Chemistry in an Oxidation Flow Reactor: Radical Formation and Recycling, Sensitivities, and OH Exposure Estimation Equation, *J. Phys. Chem. A*, 119, 4418–4432, doi:10.1021/jp509534k, 2015.
- Li, Y. J., Liu, P., Gong, Z., Wang, Y., Bateman, A. P., Bergoend, C., Bertram, A. K., and Martin, S. T.: Chemical Reactivity and Liquid/Nonliquid States of Secondary Organic Material, *Environ. Sci. Technol.*, 49, 13264–13274, doi:10.1021/acs.est.5b03392, 2015.
- Liao, J., Froyd, K. D., Murphy, D. M., Keutsch, F. N., Yu, G., Wennberg, P. O., St. Clair, J. M., Crounse, J. D., Wisthaler, A., Mikoviny, T., Jimenez, J. L., Campuzano Jost, P., Day, D. A., Hu, W., Ryerson, T. B., Pollack, I. B., Peischl, J., Anderson, B. E., Ziemba, L. D., Blake, D. R., Meinardi, S., and Diskin, G.: Airborne measurements of organosulfates over the continental US, *J. Geophys. Res.*, 120, 2990–3005, doi:10.1002/2014jd022378, 2015.
- Lin, Y.-H., Zhang, Z., Docherty, K. S., Zhang, H., Budisulistiorini, S. H., Rubitschun, C. L., Shaw, S. L., Knipping, E. M., Edgerton, E. S., Kleindienst, T. E., Gold, A., and Surratt, J. D.: Isoprene Epoxydiols as Precursors to Secondary Organic Aerosol Formation: Acid-Catalyzed Reactive Uptake Studies with Authentic Compounds, *Environ. Sci. Technol.*, 46, 250–258, doi:10.1021/es202554c, 2012.
- Lin, Y.-H., Budisulistiorini, S. H., Chu, K., Siejack, R. A., Zhang, H., Riva, M., Zhang, Z., Gold, A., Kautzman, K. E., and Surratt, J. D.: Light-Absorbing Oligomer Formation in Secondary Organic Aerosol from Reactive Uptake of Isoprene Epoxydiols, *Environ. Sci. Technol.*, 48, 12012–12021, doi:10.1021/es503142b, 2014.
- Liu, Y., Ivanov, A. V., Zelenov, V. V., and Molina, M. J.: Temperature dependence of OH uptake by carbonaceous surfaces of atmospheric importance, *Russ. J. Phys. Chem. B*, 6, 327–332, doi:10.1134/s199079311202008x, 2012.
- Lopez-Hilfiker, F., Mohr, C., D'Ambro, E. L., Lutz, A., Riedel, T. P., Gaston, C. J., Iyer, S., Zhang, Z., Gold, A., Surratt, J. D., Lee, B. H., Kurtén, T., Hu, W., Jimenez, J. L., Hallquist, M., and Thornton, J. A.: Molecular composition and volatility of organic aerosol in the Southeastern U.S.: implications for IEPOX derived SOA, *Environ. Sci. Technol.*, 50, 2200–2209, doi:10.1021/acs.est.5b04769, 2016.
- Mao, J., Ren, X., Brune, W. H., Olson, J. R., Crawford, J. H., Fried, A., Huey, L. G., Cohen, R. C., Heikes, B., Singh, H. B., Blake, D. R., Sachse, G. W., Diskin, G. S., Hall, S. R., and Shetter, R. E.: Airborne measurement of OH reactivity during INTEX-B, *Atmos. Chem. Phys.*, 9, 163–173, doi:10.5194/acp-9-163-2009, 2009.
- Marais, E. A., Jacob, D. J., Jimenez, J. L., Campuzano-Jost, P., Day, D. A., Hu, W., Krechmer, J., Zhu, L., Kim, P. S., Miller, C. C., Fisher, J. A., Travis, K., Yu, K., Hanisco, T. F., Wolfe, G. M., Arkinson, H. L., Pye, H. O. T., Froyd, K. D., Liao, J., and McNeill, V. F.: Aqueous-phase mechanism for secondary organic aerosol formation from isoprene: application to the southeast United States and co-benefit of SO<sub>2</sub> emission controls, *Atmos. Chem. Phys.*, 16, 1603–1618, doi:10.5194/acp-16-1603-2016, 2016.
- Martin, S. T., Andreae, M. O., Althausen, D., Artaxo, P., Baars, H., Borrmann, S., Chen, Q., Farmer, D. K., Guenther, A., Gunthe, S. S., Jimenez, J. L., Karl, T., Longo, K., Manzi, A., Müller, T., Pauliquevis, T., Petters, M. D., Prenni, A. J., Pöschl, U., Rizzo, L. V., Schneider, J., Smith, J. N., Swietlicki, E., Tota, J., Wang, J., Wiedensohler, A., and Zorn, S. R.: An overview of the Amazonian Aerosol Characterization Experiment 2008 (AMAZE-08), *Atmos. Chem. Phys.*, 10, 11415–11438, doi:10.5194/acp-10-11415-2010, 2010.
- Martin, S. T., Artaxo, P., Machado, L. A. T., Manzi, A. O., Souza, R. A. F., Schumacher, C., Wang, J., Andreae, M. O., Barbosa, H. M. J., Fan, J., Fisch, G., Goldstein, A. H., Guenther, A., Jimenez, J. L., Pöschl, U., Silva Dias, M. A., Smith, J. N., and Wendisch, M.: Introduction: Observations and Modeling of the Green Ocean

- Amazon (GoAmazon2014/5), *Atmos. Chem. Phys.*, 16, 4785–4797, doi:10.5194/acp-16-4785-2016, 2016.
- May, A. A., Levin, E. J. T., Hennigan, C. J., Riipinen, I., Lee, T., Collett, J. L., Jimenez, J. L., Kreidenweis, S. M., and Robinson, A. L.: Gas-particle partitioning of primary organic aerosol emissions: 3. Biomass burning, *J. Geophys. Res.*, 118, 11327–31138, doi:10.1002/jgrd.50828, 2013.
- McNeill, V. F., Yatavelli, R. L. N., Thornton, J. A., Stipe, C. B., and Landgrebe, O.: Heterogeneous OH oxidation of palmitic acid in single component and internally mixed aerosol particles: vaporization and the role of particle phase, *Atmos. Chem. Phys.*, 8, 5465–5476, doi:10.5194/acp-8-5465-2008, 2008.
- Meng, Z. and Seinfeld, J. H.: On the Source of the Submicrometer Droplet Mode of Urban and Regional Aerosols, *Aerosol. Sci. Tech.*, 20, 253–265, doi:10.1080/02786829408959681, 1994.
- Nguyen, T. B., Coggon, M. M., Bates, K. H., Zhang, X., Schwantes, R. H., Schilling, K. A., Loza, C. L., Flagan, R. C., Wennberg, P. O., and Seinfeld, J. H.: Organic aerosol formation from the reactive uptake of isoprene epoxydiols (IEPOX) onto non-acidified inorganic seeds, *Atmos. Chem. Phys.*, 14, 3497–3510, doi:10.5194/acp-14-3497-2014, 2014.
- Nguyen, T. B., Crouse, J. D., Teng, A. P., St. Clair, J. M., Paulot, F., Wolfe, G. M., and Wennberg, P. O.: Rapid deposition of oxidized biogenic compounds to a temperate forest, *Proc. Natl. Acad. Sci. USA*, 112, E392–E401, doi:10.1073/pnas.1418702112, 2015.
- Nguyen, T. K. V., Petters, M. D., Suda, S. R., Guo, H., Weber, R. J., and Carlton, A. G.: Trends in particle-phase liquid water during the Southern Oxidant and Aerosol Study, *Atmos. Chem. Phys.*, 14, 10911–10930, doi:10.5194/acp-14-10911-2014, 2014.
- Ortega, A. M., Hayes, P. L., Peng, Z., Palm, B. B., Hu, W., Day, D. A., Li, R., Cubison, M. J., Brune, W. H., Graus, M., Warneke, C., Gilman, J. B., Kuster, W. C., de Gouw, J., Gutiérrez-Montes, C., and Jimenez, J. L.: Real-time measurements of secondary organic aerosol formation and aging from ambient air in an oxidation flow reactor in the Los Angeles area, *Atmos. Chem. Phys.*, 16, 7411–7433, doi:10.5194/acp-16-7411-2016, 2016.
- Paatero, P.: User's guide for positive matrix factorization programs PMF2.EXE and PMF3.EXE, University of Helsinki, Finland, 2007.
- Pajunaja, A., Hu, W., Leong, Y. J., Taylor, N. F., Miettinen, P., Palm, B. B., Mikkonen, S., Collins, D. R., Jimenez, J. L., and Virtanen, A.: Phase state of ambient aerosol linked with water uptake and chemical aging in the Southeastern US, *Atmos. Chem. Phys. Discuss.*, doi:10.5194/acp-2016-375, in review, 2016.
- Palm, B. B., Campuzano-Jost, P., Ortega, A. M., Day, D. A., Kaser, L., Jud, W., Karl, T., Hansel, A., Hunter, J. F., Cross, E. S., Kroll, J. H., Peng, Z., Brune, W. H., and Jimenez, J. L.: In situ secondary organic aerosol formation from ambient pine forest air using an oxidation flow reactor, *Atmos. Chem. Phys.*, 16, 2943–2970, doi:10.5194/acp-16-2943-2016, 2016.
- Pankow, J. F. and Asher, W. E.: SIMPOL.1: a simple group contribution method for predicting vapor pressures and enthalpies of vaporization of multifunctional organic compounds, *Atmos. Chem. Phys.*, 8, 2773–2796, doi:10.5194/acp-8-2773-2008, 2008.
- Park, J.-H., Ivanov, A. V., and Molina, M. J.: Effect of Relative Humidity on OH Uptake by Surfaces of Atmospheric Importance, *J. Phys. Chem. A*, 112, 6968–6977, doi:10.1021/jp8012317, 2008.
- Paulot, F., Crouse, J. D., Kjaergaard, H. G., Kürten, A., St. Clair, J. M., Seinfeld, J. H., and Wennberg, P. O.: Unexpected Epoxide Formation in the Gas-Phase Photooxidation of Isoprene, *Science*, 325, 730–733, doi:10.1126/science.1172910, 2009.
- Peng, Z., Day, D. A., Stark, H., Li, R., Lee-Taylor, J., Palm, B. B., Brune, W. H., and Jimenez, J. L.: HO<sub>x</sub> radical chemistry in oxidation flow reactors with low-pressure mercury lamps systematically examined by modeling, *Atmos. Meas. Tech.*, 8, 4863–4890, doi:10.5194/amt-8-4863-2015, 2015.
- Peng, Z., Day, D. A., Ortega, A. M., Palm, B. B., Hu, W., Stark, H., Li, R., Tsigaridis, K., Brune, W. H., and Jimenez, J. L.: Non-OH chemistry in oxidation flow reactors for the study of atmospheric chemistry systematically examined by modeling, *Atmos. Chem. Phys.*, 16, 4283–4305, doi:10.5194/acp-16-4283-2016, 2016.
- Phillips, S. M. and Smith, G. D.: Light Absorption by Charge Transfer Complexes in Brown Carbon Aerosols, *Environ. Sci. Technol. Lett.*, 1, 382–386, doi:10.1021/ez500263j, 2014.
- Phillips, S. M. and Smith, G. D.: Further Evidence for Charge Transfer Complexes in Brown Carbon Aerosols from Excitation–Emission Matrix Fluorescence Spectroscopy, *J. Phys. Chem. A*, 119, 4545–4551, doi:10.1021/jp510709e, 2015.
- Ranjan, M., Presto, A. A., May, A. A., and Robinson, A. L.: Temperature Dependence of Gas–Particle Partitioning of Primary Organic Aerosol Emissions from a Small Diesel Engine, *Aerosol. Sci. Tech.*, 46, 13–21, doi:10.1080/02786826.2011.602761, 2012.
- Renbaum-Wolff, L., Grayson, J. W., Bateman, A. P., Kuwata, M., Sellier, M., Murray, B. J., Shilling, J. E., Martin, S. T., and Bertram, A. K.: Viscosity of  $\alpha$ -pinene secondary organic material and implications for particle growth and reactivity, *Proc. Natl. Acad. Sci. USA*, 110, 8014–8019, doi:10.1073/pnas.1219548110, 2013.
- Riedel, T. P., Lin, Y.-H., Budisulistiorini, S. H., Gaston, C. J., Thornton, J. A., Zhang, Z., Vizuete, W., Gold, A., and Surratt, J. D.: Heterogeneous Reactions of Isoprene-Derived Epoxides: Reaction Probabilities and Molar Secondary Organic Aerosol Yield, *Environ. Sci. Technol. Lett.*, 2, 38–42, doi:10.1021/ez500406f, 2015.
- Riedel, T. P., Lin, Y.-H., Zhang, Z., Chu, K., Thornton, J. A., Vizuete, W., Gold, A., and Surratt, J. D.: Constraining condensed-phase formation kinetics of secondary organic aerosol components from isoprene epoxydiols, *Atmos. Chem. Phys.*, 16, 1245–1254, doi:10.5194/acp-16-1245-2016, 2016.
- Riva, M., Bell, D. M., Hansen, A.-M. K., Drozd, G. T., Zhang, Z., Gold, A., Imre, D., Surratt, J. D., Glasius, M., and Zelenyuk, A.: Effect of Organic Coatings, Humidity and Aerosol Acidity on Multiphase Chemistry of Isoprene Epoxydiols, *Environ. Sci. Technol.*, 50, 5580–5588, doi:10.1021/acs.est.5b06050, 2016.
- Robinson, N. H., Hamilton, J. F., Allan, J. D., Langford, B., Oram, D. E., Chen, Q., Docherty, K., Farmer, D. K., Jimenez, J. L., Ward, M. W., Hewitt, C. N., Barley, M. H., Jenkin, M. E., Rickard, A. R., Martin, S. T., McFiggans, G., and Coe, H.: Evidence for a significant proportion of Secondary Organic Aerosol from isoprene above a maritime tropical forest, *Atmos. Chem. Phys.*, 11, 1039–1050, doi:10.5194/acp-11-1039-2011, 2011.
- Sharpless, C. M. and Blough, N. V.: The importance of charge-transfer interactions in determining chromophoric dissolved organic matter (CDOM) optical and photochemi-

- cal properties, *Environ. Sci. Process. Impacts*, 16, 654–671, doi:10.1039/c3em00573a, 2014.
- Slade, J. H. and Knopf, D. A.: Heterogeneous OH oxidation of biomass burning organic aerosol surrogate compounds: assessment of volatilisation products and the role of OH concentration on the reactive uptake kinetics, *Phys. Chem. Chem. Phys.*, 15, 5898–5915, doi:10.1039/c3cp44695f, 2013.
- Slade, J. H. and Knopf, D. A.: Multiphase OH oxidation kinetics of organic aerosol: The role of particle phase state and relative humidity, *Geophys. Res. Lett.*, 41, 5297–5306, doi:10.1002/2014gl060582, 2014.
- Slowik, J. G., Wong, J. P. S., and Abbatt, J. P. D.: Real-time, controlled OH-initiated oxidation of biogenic secondary organic aerosol, *Atmos. Chem. Phys.*, 12, 9775–9790, doi:10.5194/acp-12-9775-2012, 2012.
- Smith, J. D., Kroll, J. H., Cappa, C. D., Che, D. L., Liu, C. L., Ahmed, M., Leone, S. R., Worsnop, D. R., and Wilson, K. R.: The heterogeneous reaction of hydroxyl radicals with sub-micron squalane particles: a model system for understanding the oxidative aging of ambient aerosols, *Atmos. Chem. Phys.*, 9, 3209–3222, doi:10.5194/acp-9-3209-2009, 2009.
- Song, M., Liu, P. F., Hanna, S. J., Li, Y. J., Martin, S. T., and Bertram, A. K.: Relative humidity-dependent viscosities of isoprene-derived secondary organic material and atmospheric implications for isoprene-dominant forests, *Atmos. Chem. Phys.*, 15, 5145–5159, doi:10.5194/acp-15-5145-2015, 2015.
- Surratt, J. D., Chan, A. W. H., Eddingsaas, N. C., Chan, M., Loza, C. L., Kwan, A. J., Hersey, S. P., Flagan, R. C., Wennberg, P. O., and Seinfeld, J. H.: Reactive intermediates revealed in secondary organic aerosol formation from isoprene, *Proc. Natl. Acad. Sci. USA*, 107, 6640–6645, doi:10.1073/pnas.0911114107, 2010.
- Tsigaridis, K., Daskalakis, N., Kanakidou, M., Adams, P. J., Artaxo, P., Bahadur, R., Balkanski, Y., Bauer, S. E., Bellouin, N., Benedetti, A., Bergman, T., Bernsten, T. K., Beukes, J. P., Bian, H., Carslaw, K. S., Chin, M., Curci, G., Diehl, T., Easter, R. C., Ghan, S. J., Gong, S. L., Hodzic, A., Hoyle, C. R., Iversen, T., Jathar, S., Jimenez, J. L., Kaiser, J. W., Kirkevåg, A., Koch, D., Kokkola, H., Lee, Y. H., Lin, G., Liu, X., Luo, G., Ma, X., Mann, G. W., Mihalopoulos, N., Morcrette, J.-J., Müller, J.-F., Myhre, G., Myriokefalitakis, S., Ng, N. L., O'Donnell, D., Penner, J. E., Pozzoli, L., Pringle, K. J., Russell, L. M., Schulz, M., Sciare, J., Seland, Ø., Shindell, D. T., Sillman, S., Skeie, R. B., Spracklen, D., Stavrou, T., Steenrod, S. D., Takemura, T., Tititta, P., Tilmes, S., Tost, H., van Noije, T., van Zyl, P. G., von Salzen, K., Yu, F., Wang, Z., Wang, Z., Zaveri, R. A., Zhang, H., Zhang, K., Zhang, Q., and Zhang, X.: The AeroCom evaluation and intercomparison of organic aerosol in global models, *Atmos. Chem. Phys.*, 14, 10845–10895, doi:10.5194/acp-14-10845-2014, 2014.
- Ulbrich, I. M., Canagaratna, M. R., Zhang, Q., Worsnop, D. R., and Jimenez, J. L.: Interpretation of organic components from Positive Matrix Factorization of aerosol mass spectrometric data, *Atmos. Chem. Phys.*, 9, 2891–2918, doi:10.5194/acp-9-2891-2009, 2009.
- Vaden, T. D., Imre, D., Beránek, J., Shrivastava, M., and Zelenyuk, A.: Evaporation kinetics and phase of laboratory and ambient secondary organic aerosol, *Proc. Natl. Acad. Sci. USA*, 108, 2190–2195, doi:10.1073/pnas.1013391108, 2011.
- Volkamer, R., Jimenez, J. L., San Martini, F., Dzepina, K., Zhang, Q., Salcedo, D., Molina, L. T., Worsnop, D. R., and Molina, M. J.: Secondary organic aerosol formation from anthropogenic air pollution: Rapid and higher than expected, *Geophys. Res. Lett.*, 33, L17811, doi:10.1029/2006gl026899, 2006.
- Washenfelder, R. A., Attwood, A. R., Brock, C. A., Guo, H., Xu, L., Weber, R. J., Ng, N. L., Allen, H. M., Ayres, B. R., Baumann, K., Cohen, R. C., Draper, D. C., Duffey, K. C., Edgerton, E., Fry, J. L., Hu, W. W., Jimenez, J. L., Palm, B. B., Romer, P., Stone, E. A., Wooldridge, P. J., and Brown, S. S.: Biomass burning dominates brown carbon absorption in the rural southeastern United States, *Geophys. Res. Lett.*, 42, 653–664, doi:10.1002/2014gl062444, 2015.
- Weitkamp, E. A., Lambe, A. T., Donahue, N. M., and Robinson, A. L.: Laboratory Measurements of the Heterogeneous Oxidation of Condensed-Phase Organic Molecular Makers for Motor Vehicle Exhaust, *Environ. Sci. Technol.*, 42, 7950–7956, doi:10.1021/es800745x, 2008.
- Wong, J. P. S., Lee, A. K. Y., and Abbatt, J. P. D.: Impacts of Sulfate Seed Acidity and Water Content on Isoprene Secondary Organic Aerosol Formation, *Environ. Sci. Technol.*, 49, 13215–13221, doi:10.1021/acs.est.5b02686, 2015.
- Xie, Y., Paulot, F., Carter, W. P. L., Nolte, C. G., Luecken, D. J., Hutzell, W. T., Wennberg, P. O., Cohen, R. C., and Pinder, R. W.: Understanding the impact of recent advances in isoprene photooxidation on simulations of regional air quality, *Atmos. Chem. Phys.*, 13, 8439–8455, doi:10.5194/acp-13-8439-2013, 2013.
- Xu, L., Guo, H., Boyd, C. M., Klein, M., Bougiatioti, A., Cerully, K. M., Hite, J. R., Isaacman-VanWertz, G., Kreisberg, N. M., Knote, C., Olson, K., Koss, A., Goldstein, A. H., Hering, S. V., de Gouw, J., Baumann, K., Lee, S.-H., Nenes, A., Weber, R. J., and Ng, N. L.: Effects of anthropogenic emissions on aerosol formation from isoprene and monoterpenes in the southeastern United States, *Proc. Natl. Acad. Sci. USA*, 112, 37–42, doi:10.1073/pnas.1417609112, 2014.
- Zhang, Q., Jimenez, J. L., Canagaratna, M. R., Allan, J. D., Coe, H., Ulbrich, I., Alfarra, M. R., Takami, A., Middlebrook, A. M., Sun, Y. L., Dzepina, K., Dunlea, E., Docherty, K., DeCarlo, P. F., Salcedo, D., Onasch, T., Jayne, J. T., Miyoshi, T., Shimojo, A., Hatakeyama, S., Takegawa, N., Kondo, Y., Schneider, J., Drewnick, F., Borrmann, S., Weimer, S., Demerjian, K., Williams, P., Bower, K., Bahreini, R., Cottrell, L., Griffin, R. J., Rautiainen, J., Sun, J. Y., Zhang, Y. M., and Worsnop, D. R.: Ubiquity and dominance of oxygenated species in organic aerosols in anthropogenically-influenced Northern Hemisphere midlatitudes, *Geophys. Res. Lett.*, 34, L13801, doi:10.1029/2007gl029979, 2007.